

AD-A067 324

NAVAL OCEAN SYSTEMS CENTER SAN DIEGO CA

F/G 12/1

SPECTRAL ESTIMATION USING POISSON DISTRIBUTED TIME SERIES DATA --ETC(U)

OCT 78 C MIRABILE

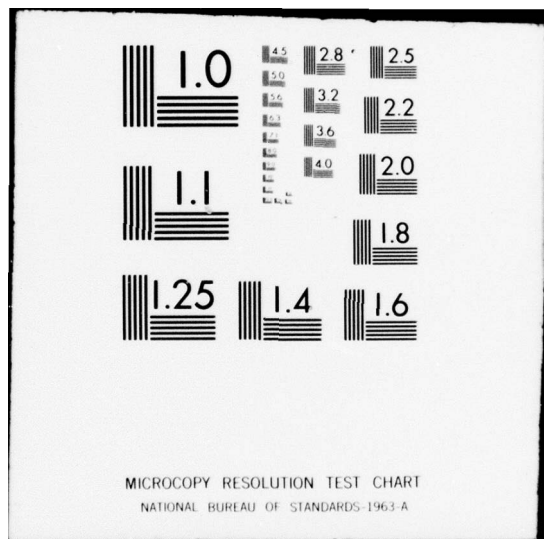
UNCLASSIFIED

NOSC/TR-325

NL

| OF |
AD
A067324





AD A0 67324

LEVEL

12
na

NOSC

NOSC TR 325

DDC
RECEIVED
APR 17 1979
CH

NOSC TR 325

Technical Report 325

SPECTRAL ESTIMATION USING POISSON DISTRIBUTED TIME SERIES DATA WITH TIME QUANTIZATION

C Mirabile

15 October 1978

Final Report: October 1977 - September 1978

DDC FILE COPY

Approved for public release; distribution unlimited

NAVAL OCEAN SYSTEMS CENTER
SAN DIEGO, CALIFORNIA 92152

79 04 10 013



NAVAL OCEAN SYSTEMS CENTER, SAN DIEGO, CA 92152

AN ACTIVITY OF THE NAVAL MATERIAL COMMAND

RR GAVAZZI, CAPT, USN

Commander

HL BLOOD

Technical Director

ADMINISTRATIVE INFORMATION

This work, accomplished during fiscal year 1978, was funded by the Independent Research (IR) program of the Naval Ocean Systems Center, and was part of the Random Sampling Techniques for Spectral Estimation program (ZR24718).

Released by
D. A. Hanna, Head
Signal Processing and Display
Division

Under authority of
H. A. Schenck, Head
Undersea Surveillance Department

ACKNOWLEDGMENT

The excellent computer programming support for this program, provided by B. Kuey, who is working at NOSC through the San Diego State Foundation, is greatly appreciated.

UNCLASSIFIED

SECURITY CLASSIFICATION OF THIS PAGE (When Data Entered)

REPORT DOCUMENTATION PAGE		READ INSTRUCTIONS BEFORE COMPLETING FORM
1. REPORT NUMBER NOSC/TR-325	2. GOVT ACCESSION NO.	3. RECIPIENT'S CATALOG NUMBER
4. TITLE (and Subtitle) SPECTRAL ESTIMATION USING POISSON DISTRIBUTED TIME SERIES DATA WITH TIME QUANTIZATION,	5. TYPE OF REPORT & PERIOD COVERED Final Report. EX-1078 Oct 77 - Sep 78	
7. AUTHOR(s) C. Mirabile	8. CONTRACT OR GRANT NUMBER(s)	
9. PERFORMING ORGANIZATION NAME AND ADDRESS Naval Ocean Systems Center San Diego, California 92152	10. PROGRAM ELEMENT, PROJECT, TASK AREA & WORK UNIT NUMBERS ZR24718	
11. CONTROLLING OFFICE NAME AND ADDRESS Naval Ocean Systems Center San Diego, California 92152	12. REPORT DATE 15 October 1978	13. NUMBER OF PAGES 42
14. MONITORING AGENCY NAME & ADDRESS (if different from Controlling Office) 1245p.	15. SECURITY CLASS. (of this report) Unclassified	
16. DISTRIBUTION STATEMENT (of this Report) Approved for public release; distribution unlimited.		
17. DISTRIBUTION STATEMENT (of the abstract entered in Block 20, if different from Report) D D C RECEIVED APR 17 1979 RECEIVED G		
18. SUPPLEMENTARY NOTES		
19. KEY WORDS (Continue on reverse side if necessary and identify by block number) Spectral estimation Poisson sampling		
20. ABSTRACT (Continue on reverse side if necessary and identify by block number) In this report spectral estimation, using Poisson distributed time samples which have been time quantized, is considered. An expression for the probability density function for the time quantized Poisson samples is derived. For a large class of nonbandlimited spectral density functions the bias of the spectral estimates is determined and an asymptotic bound on the variance is also derived. Numerical analysis of the bias and variance bound is performed and graphs of the bias as a function of frequency are presented. Finally, examples of spectral estimates are given with varying degrees of time quantization. Results show small amount of bias introduced into estimates and variance remains almost unaffected. The chief advantage of Poisson sampling theory is		

DD FORM 1473 1 JAN 73

EDITION OF 1 NOV 65 IS OBSOLETE
S/N 0102-LF-014-6601

UNCLASSIFIED

SECURITY CLASSIFICATION OF THIS PAGE (When Data Entered)

393 159

LB

UNCLASSIFIED

SECURITY CLASSIFICATION OF THIS PAGE (When Data Entered)

20. Abstract (Continued)

that it eliminates spectral aliasing on nonbandlimited and undersampled time series data. Time quantized Poisson data results from sampling constraints due to hardware implementation.

UNCLASSIFIED

SECURITY CLASSIFICATION OF THIS PAGE(When Data Entered)

CONTENTS

- I. INTRODUCTION . . . page 3
- II. THEORY . . . 4
Statistics for the Time Quantized Spectral Estimator . . . 6
- III. NUMERICAL AND SIMULATION RESULTS . . . 13
- IV. CONCLUSIONS . . . 25
- V. APPENDIX . . . 27
- VI. REFERENCES . . . 42

APPROVED FOR	BY	DATE
NO. OF	NO. OF	
CUSTOMER'S NAME AND ADDRESS		
CITY		
STATE		
ZIP		
TELEPHONE		
FACSIMILE		
ELECTRONIC MAIL		
OTHER		
REMARKS		
A		

TABLES

1. Numerical results showing second moment component bounds of spectral estimator $\hat{\varphi}_N(\lambda)$ and the asymptotic variance bound of estimator for $\beta = 1.0$ rad/sec, $\epsilon = 0.0001$. . . page 20
2. Numerical results showing second moment component bounds of spectral estimator $\hat{\varphi}_N(\lambda)$ and the asymptotic variance bound of estimator for $\beta = 1.0$ rad/sec, $\epsilon = 0.01$. . . 21
3. Numerical results showing second moment component bounds of spectral estimator $\hat{\varphi}_N(\lambda)$ and the asymptotic variance bound of estimator for $\beta = 10.0$ rad/sec, $\epsilon = 0.001$. . . 21
4. Numerical results showing second moment component bounds of spectral estimator $\hat{\varphi}_N(\lambda)$ and the asymptotic variance bound of estimator for $\beta = 10.0$ rad/sec, $\epsilon = 0.1$. . . 22

FIGURES

1. Probability density function for time-quantized Poisson distributed events where $\beta = 10$ rad/sec, and $\epsilon = 0.01$. . . page 7
2. Spectral density function simulated for numerical analysis . . . 13
3. Bias of time-quantized Poisson spectral estimate as a function of frequency for $\beta = 1$ rad/sec, $N = 1000$ and $M_N = 7$. . . 14
4. Percent bias of time-quantized Poisson spectral estimate as a function of frequency and epsilon for $\beta = 1$ rad/sec, $N = 1000$, and $M_N = 7$. . . 15
5. Bias of time-quantized Poisson spectral estimate as a function of frequency and epsilon for $\beta = 5$ rad/sec, $N = 1000$ and $M_N = 6$. . . 16
6. Percent bias of time-quantized spectral estimate as a function of frequency and epsilon for $\beta = 5$ rad/sec, $N = 1000$ and $M_N = 6$. . . 17
7. Bias of time-quantized spectral estimate as a function of frequency and epsilon for $\beta = 10$ rad/sec, $N = 1000$ and $M_N = 6$. . . 18
8. Percent bias of time-quantized spectral estimate as a function of frequency and epsilon for $\beta = 10$ rad/sec, $N = 1000$ and $M_N = 6$. . . 19
9. Spectral estimate for $\beta = 1$ rad/sec, $M_N = 7$ and several values of epsilon . . . 23
10. Spectral estimate for $\beta = 5$ rad/sec, $M_N = 6$ and several values of epsilon . . . 23
11. Spectral estimate for $\beta = 10$ rad/sec, $M_N = 6$ and several values of epsilon . . . 24

79 04¹ 10 013

SUMMARY

In this report spectral estimation, using Poisson distributed time samples which have been time quantized, is considered. An expression for the probability density function for the time quantized Poisson samples is derived. For a large class of nonbandlimited spectral density functions the bias of the spectral estimates is determined and an asymptotic bound on the variance is also derived. Numerical analysis of the bias and variance bound is performed and graphs of the bias as a function of frequency are presented. Finally, examples of spectral estimates are given with varying degrees of time quantization. Results show small amount of bias introduced into estimates and variance remains almost unaffected. The chief advantage of Poisson sampling theory is that it eliminates spectral aliasing on nonbandlimited and undersampled time series data. Time quantized Poisson data results from sampling constraints due to hardware implementation.

I. INTRODUCTION

Spectral estimation is a widely used method in the analysis of ocean data. Typically, continuous time-data are sampled with equally spaced data points and the spectral density function is then estimated via the discrete Fourier transform (DFT). A new approach has been proposed for certain applications which use sample points that are Poisson distributed in time [1, 2]. The chief advantage of this approach is that it has been shown to be alias free both by theoretical means [3] and by simulation [2].

In this report we consider Poisson distributed samples of a continuous time signal which have been time quantized. Time quantization for the Poisson case can be explained as follows. The random nature of the Poisson distributed sample points provides a probability that two data points may be spaced arbitrarily close in time. If one were attempting to sample real world data with Poisson distributed data points the sampling device would most likely be limited in the speed it could extract data samples. Thus, whenever the Poisson distribution required two events or sample points to come some small epsilon (ϵ) apart, the sampling device would be unable to respond in time to collect both samples. This epsilon will be referred to as the "quantization."

There are several cases of time quantization which could be developed, some of which are listed below.

1. If an event occurs during the quantization time interval of the processor, it has no effect whatsoever.
2. If an event occurs during the quantization time, it starts quantization time over again.
3. If an event occurs during the quantization time, it starts the quantization time over again with probability p .
4. The value of the quantization time (ϵ) is added to the interval after each event whether the event occurs during the quantization time or not.

The first three cases are very difficult problems to investigate analytically because the time intervals between events would not be independent. The fourth case is the simplest and is the focus of the work reported here.

In the following section the probability density function for the sampling times is derived. In addition, using the spectral estimator proposed in [1] and assuming time quantized sample times, an exact expression for the bias of the estimator is derived for a large class of spectral density functions. Finally, for the same class of spectral density functions, an upper bound on the variance of the spectral estimator of [1] is derived and its properties examined.

Section III demonstrates the behavior of time quantized data in performing spectral estimation with examples of estimation of a first order Gauss-Markov spectral density using data with various degrees of time quantization. In addition, the behavior of the bias expression is examined numerically with graphs describing bias as a function of frequency for several different situations. Finally, in this section the behavior of the variance bound is examined. Conclusions and a discussion of the time quantization problem are included in section IV.

II. THEORY

In this section a derivation of the probability density function for the time quantized sampling times is presented. Also determined are the bias and a bound for the variance of the spectral estimator of [1] for time quantized Poisson sampled data.

Let $X = \{X(t), -\infty < t < \infty\}$ be a continuous parameter zero mean, second order, stationary random process with correlation function $C(t) \in L_1$ and spectral density function $\varphi(\lambda)$ given by

$$\varphi(\lambda) = \int_{-\infty}^{\infty} C(t) e^{-i\lambda t} \frac{dt}{2\pi} \quad (1)$$

The time quantized sampling instants are driven by a Poisson point process and are given by

$$\begin{aligned} t_0 &= 0 \\ t_n &= t_{n-1} + \alpha_n + \epsilon \quad n = 1, 2, \dots \end{aligned}$$

where the $\{\alpha_n\}$ are independent identically distributed random variables with a common exponential distribution $F(x) = 1 - e^{-\beta x}$. It is assumed that the sampling instants $\{t_n\}_{n=0}^{\infty}$ are independent of the process X . Note that β is the average sampling rate and as shown in [1], almost every realization of a Poisson point process has a density of points β . The effect of the quantization (ϵ) on the sequence $\{t_n\}$ is to enlarge each interval by ϵ and therefore shift the n^{th} sample time t_n by $n\epsilon$.

Given the observation $\{X(t_k)\}_{k=1}^N$ we will consider the estimate $\hat{\varphi}_N(\lambda)$ of the spectral density $\varphi(\lambda)$ as proposed in [1]:

$$\hat{\varphi}_N(\lambda) = \frac{1}{\pi\beta N} \sum_{n=1}^{M_N} \sum_{k=1}^{N-n} X(t_{k+n}) X(t_k) \cos \lambda(t_{k+n} - t_k) \quad (2)$$

where $M_N > 0$ is such that $M_N \rightarrow \infty$ and $M_N/N \rightarrow 0$ as $N \rightarrow \infty$.

The following Lemma will be needed in the proof of the bias and variance of the time quantized spectral estimate (2).

Lemma 1: Consider the probability density function for the distribution of the intervals of a Poisson process.

$$f_s(s) = \beta e^{-\beta s} U(s)$$

where $U(\cdot)$ is the unit step function. If the probability density function for intervals of a Poisson process that have been quantized or time expanded by an amount ϵ is

$$f_s(s) = \beta e^{-\beta(s-\epsilon)} U(s-\epsilon) ,$$

then the probability density function for the time quantized Poisson distributed sampling times $\{t_n\}$ is given by

$$f_{t_n}(t) = \beta^n \frac{(t - \epsilon n)^{n-1}}{(n-1)!} e^{-\beta(t - \epsilon n)} U(t - \epsilon n) \quad (3)$$

Proof: Since the intervals $\{s_i\}$ of a Poisson process are independent, the sampling times $\{t_n\}$ can be represented by a sum of independent, identically distributed random variables. If each interval is quantized by an epsilon, we then have

$$\begin{aligned} t_1 &= s_1 + \epsilon \\ t_2 &= s_1 + s_2 + 2\epsilon \\ t_3 &= s_1 + s_2 + s_3 + 3\epsilon \\ &\vdots \\ t_n &= \sum_{i=1}^n s_i + n\epsilon . \end{aligned}$$

Now the characteristic function of the time quantized intervals can be expressed as:

$$\begin{aligned} \varphi_t(\omega) &= \int_{-\infty}^{\infty} U(s - \epsilon) \beta e^{-\beta(s - \epsilon)} e^{i\omega s} ds \\ &= \left(\frac{\beta}{\beta - i\omega} \right) e^{i\epsilon\omega} . \end{aligned}$$

The characteristic function of the n^{th} sample time $\varphi_{t_n}(\omega)$ will then be:

$$\varphi_{t_n}(\omega) = [\varphi_t(\omega)]^n = \left(\frac{\beta}{\beta - i\omega} \right)^n e^{i\epsilon\omega n} .$$

Finally, the density function $f_{t_n}(t)$ is the inverse Fourier transform of $\varphi_{t_n}(\omega)$

$$\begin{aligned} f_{t_n}(t) &= \int_{-\infty}^{\infty} \left(\frac{\beta}{\beta - i\omega} \right)^n e^{-i\omega(t - \epsilon n)} d\omega \\ &= \beta^n \frac{(t - \epsilon n)^{n-1}}{(n-1)!} e^{-\beta(t - \epsilon n)} U(t - \epsilon n). \quad \epsilon \geq 0 \end{aligned}$$

Q.E.D.

It is easily seen that $f_{t_n}(t)$ satisfies the properties of a probability density function [4] namely

$$\begin{aligned} f_{t_n}(t) &\geq 0 \quad \forall t \\ \int_{-\infty}^{\infty} f_{t_n}(t) dt &= 1 \end{aligned}$$

Figure 1 is a graph representing the probability density function $f_{t_n}(t)$ as a function of time for several values of n .

STATISTICS OF THE SPECTRAL ESTIMATOR FOR THE TIME QUANTIZED CASE

Here we assume that the process X is a stationary, Gaussian process. For a large class of spectral densities we will present an expression for the bias and a bound for the variance of the spectral estimator (2) for time quantized sample points.

Let the covariance function $C(t)$ have the following form

$$C(\tau) = A e^{-\alpha|\tau|} \quad (4)$$

with corresponding spectral density function

$$\varphi(\lambda) = \frac{A}{\pi} \left(\frac{\alpha}{\alpha^2 + \lambda^2} \right) \quad (5)$$

where A and α are fixed positive constant parameters, and define the bias of the estimate (2) to be

$$b[\hat{\varphi}_N(\lambda)] = E[\hat{\varphi}_N(\lambda)] - \varphi(\lambda).$$

Theorem 1: Let the covariance function $C(t)$ be given by (4), then the bias of the estimate (2) for the time quantization ϵ is equal to:

$$b[\hat{\varphi}_N(\lambda)] = \frac{A}{\pi\beta} \sum_{n=1}^{M_N} \left(1 - \frac{n}{N} \right) (\beta e^{-\epsilon\alpha})^n [(\alpha + \beta)^2 + \lambda^2]^{-n/2} \cdot \cos \left[(\lambda\epsilon n) + n \tan^{-1} \left(\frac{\lambda}{\alpha + \beta} \right) \right] - \frac{A}{\pi} \left(\frac{\alpha}{\alpha^2 + \lambda^2} \right). \quad (6)$$

Proof: Let E_X and $E_{\{t_n\}}$ represent expectation with respect to X and $\{t_n\}$. Then

$$\begin{aligned} b[\hat{\varphi}_N(\lambda)] &= E_{\{t_n\}} E_X \left\{ \frac{A}{\pi\beta N} \sum_{n=1}^{M_N} \sum_{k=1}^{N-n} X(t_{k+n}) X(t_k) \cos \lambda (t_{k+n} - t_k) \right\} - \varphi(\lambda) \\ &= \frac{A}{\pi\beta N} \sum_{n=1}^{M_N} (N-n) \int_0^{\infty} C(t) \cos(\lambda t) f_{t_n}(t) dt - \frac{A}{\pi} \left(\frac{\alpha}{\alpha^2 + \lambda^2} \right) \end{aligned}$$

where $f_{t_n}(t)$ is given by (3). Substituting for $C(t)$ and $f_{t_n}(t)$ we then have

$$\begin{aligned} &= \frac{A}{\pi\beta N} \sum_{n=1}^{M_N} (N-n) \int_{n\epsilon}^{\infty} e^{-\alpha t} \cos(\lambda t) \frac{(t - \epsilon n)^{n-1}}{(n-1)!} \beta^n e^{-\beta(t - \epsilon n)} dt \\ &\quad - \frac{A}{\pi} \left(\frac{\alpha}{\alpha^2 + \lambda^2} \right) \end{aligned}$$

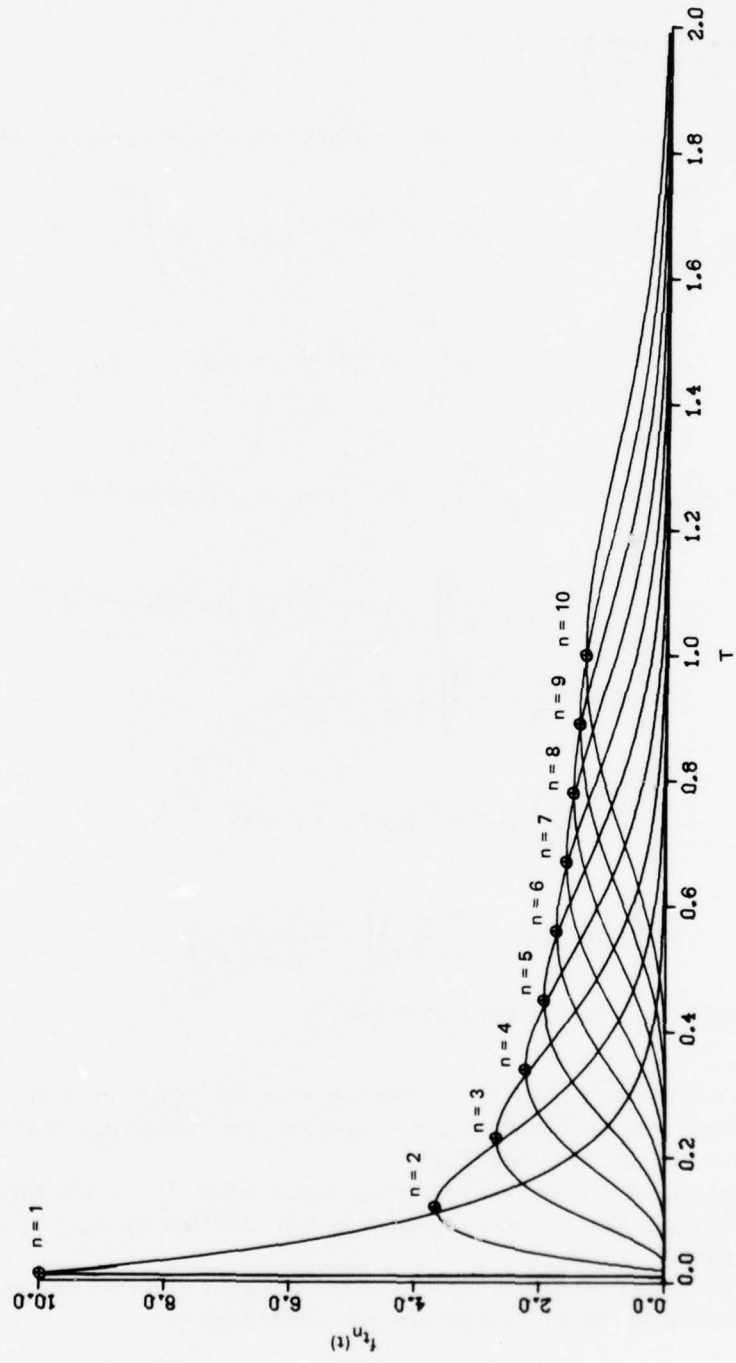


Figure 1. Probability density function for time-quantized Poisson distributed events where $\beta = 10$ rad/sec, and $\epsilon = 0.01$.

$$= \frac{A}{\pi\beta N} \sum_{n=1}^{M_N} (N-n) \frac{\beta^n}{(n-1)!} e^{\beta\epsilon n} \int_0^\infty e^{-(u+\epsilon n)(\beta+\alpha)} \cos \lambda(u+\epsilon n) u^{n-1} du$$

$$- \frac{A}{\pi} \left(\frac{\alpha}{\alpha^2 + \lambda^2} \right)$$

by a change of variable $u = t - n\epsilon$. Next expand the cosine function to give

$$\frac{A}{\pi\beta N} \sum_{n=1}^{M_N} (N-n) \frac{\beta^n}{(n-1)!} e^{\beta\epsilon n} e^{-\epsilon n(\beta+\alpha)} \left\{ \cos(\lambda\epsilon n) \int_0^\infty e^{-u(\beta+\alpha)} \cos(\lambda u) \right.$$

$$\cdot u^{n-1} du - \sin(\lambda\epsilon n) \int_0^\infty e^{-u(\beta+\alpha)} \sin(\lambda u) u^{n-1} du \left. \right\} - \frac{A}{\pi} \left(\frac{\alpha}{\alpha^2 + \lambda^2} \right)$$

$$= \frac{A}{\pi\beta N} \sum_{n=1}^{M_N} (N-n) \frac{\beta^n}{(n-1)!} e^{-\epsilon n\alpha} \left\{ \cos(\lambda\epsilon n) \Gamma(n) [(\alpha+\beta)^2 + \lambda^2]^{-n/2} \right.$$

$$\cdot \cos \left[n \tan^{-1} \left(\frac{\lambda}{\alpha+\beta} \right) \right] - \sin(\lambda\epsilon n) \Gamma(n) [(\alpha+\beta)^2 + \lambda^2]^{-n/2}$$

$$\cdot \sin \left[n \tan^{-1} \left(\frac{\lambda}{\alpha+\beta} \right) \right] \left. \right\} - \frac{A}{\pi} \frac{\alpha}{\alpha^2 + \lambda^2}$$

$$= \frac{A}{\pi\beta} \sum_{n=1}^{M_N} \left(1 - \frac{n}{N} \right) (\beta e^{-\epsilon\alpha})^n [(\alpha+\beta)^2 + \lambda^2]^{-n/2}$$

$$\cdot \cos \left[\lambda\epsilon n + n \tan^{-1} \left(\frac{\lambda}{\alpha+\beta} \right) \right] - \frac{A}{\pi} \left(\frac{\alpha}{\alpha^2 + \lambda^2} \right)$$

where the integrals were evaluated using [5].

Q.E.D.

An examination of (6) reveals that since the first few terms in the summation are dominant there is not a high dependence on N and M_N . We see also that the bias decreases as λ increases at a rate of at least $1/\lambda$.

Next we consider the variance of the estimate (2). We assume that the process X is stationary to order four and has covariance and spectral density functions as given in (4) and (5), respectively.

In the derivation of the variance bound we begin with the same procedure as in [1]. Consider the fourth order cumulant function defined by

$$Q(\tau_1, \tau_2, \tau_3) = E[X(t) X(t + \tau_1) X(t + \tau_2) X(t + \tau_3)]$$

$$- C(\tau_1) C(\tau_3 - \tau_2) - C(\tau_2) C(\tau_1 - \tau_3) - C(\tau_3) C(\tau_2 - \tau_1) \quad (7)$$

where X and $C(\tau)$ are as previously defined.

If we assume the process X to be Gaussian, then (7) becomes

$$E[X(t) X(t + \tau_1) X(t + \tau_2) X(t + \tau_3)] = C(\tau_1) C(\tau_3 - \tau_2) + C(\tau_2) C(\tau_1 - \tau_3) \\ + C(\tau_3) C(\tau_2 - \tau_1).$$

Now, we look at the second moment of the estimate (2)

$$E[\hat{\varphi}_N^2(\lambda)] = \frac{1}{(\pi\beta N)^2} \sum_{n=1}^{M_N} \sum_{n'=1}^{M_N} \sum_{k=1}^{N-n} \sum_{k'=1}^{N-n'} E_{\{t_n\}} \left\{ C(t_{k+n} - t_k) C(t_{k'+n'} - t_{k'}) \right. \\ \left. + C(t_{k'} - t_k) C(t_{k+n} - t_{k'+n'}) + C(t_{k'+n'} - t_k) C(t_{k'} - t_{k+n}) \right\} \\ \cdot \cos \lambda(t_{k+n} - t_k) \cos \lambda(t_{k'+n'} - t_{k'}). \quad (8)$$

The expectation with respect to t_n in (8) makes its solution very difficult to obtain. In order to solve the expectation in (8) and bound the variance of (2) we will break the summations up and evaluate them in eleven disjoint regions corresponding to the different permutations of

$\{k, k', k+n, k'+n'\}$.

Let $E[\hat{\varphi}_N(\lambda)]^2$ be divided into the following three expressions

$$E[\hat{\varphi}_N(\lambda)]^2 = \sum_{i=1}^3 U_i(\lambda)$$

where

$$U_1(\lambda) = \frac{1}{(\pi\beta N)^2} \sum_{n=1}^{M_N} \sum_{n'=1}^{M_N} \sum_{k=1}^{N-n} \sum_{k'=1}^{N-n'} E_{t_n} \left\{ C(t_{k+n} - t_k) C(t_{k'+n'} - t_{k'}) \right. \\ \left. \cdot \cos \lambda(t_{k+n} - t_k) \cos \lambda(t_{k'+n'} - t_{k'}) \right\} \quad (9)$$

$$U_2(\lambda) = \frac{1}{(\pi\beta N)^2} \sum_{n=1}^{M_N} \sum_{n'=1}^{M_N} \sum_{k=1}^{N-n} \sum_{k'=1}^{N-n'} E_{t_n} \left\{ C(t_{k'} - t_k) C(t_{k+n} - t_{k'+n'}) \right. \\ \left. \cdot \cos \lambda(t_{k+n} - t_k) \cos \lambda(t_{k'+n'} - t_{k'}) \right\} \quad (10)$$

$$U_3(\lambda) = \frac{1}{(\pi\beta N)^2} \sum_{n=1}^{M_N} \sum_{n'=1}^{M_N} \sum_{k=1}^{N-n} \sum_{k'=1}^{N-n'} E_{t_n} \left\{ C(t_{k'+n'} - t_k) C(t_{k'} - t_{k+n}) \right. \\ \left. \cdot \cos \lambda(t_{k+n} - t_k) \cos \lambda(t_{k'+n'} - t_{k'}) \right\}. \quad (11)$$

Lemma 2: If the process X is Gaussian and has a covariance function given by (4) then an upper bound on $U_1(\lambda)$ is given by:

$$\begin{aligned}
U_1(\lambda) \leq Y_1(\lambda) &= \frac{A^2}{(\pi\beta N)^2} \sum_{n=1}^{M_N} (N-n) W^{2n} + \frac{2A^2}{(\pi\beta N)^2} \\
&\cdot \left\{ \frac{1}{4} \sum_{n=1}^{M_N} \sum_{n'=1}^{M_N} \beta^{n+n'} \operatorname{Rl} \left(\frac{e^{-\epsilon[\alpha-i\lambda]}}{[(\alpha+\beta)-i\lambda]} \right)^n \operatorname{Rl} \left(\frac{e^{-\epsilon[\alpha-i\lambda]}}{[(\alpha+\beta)-i\lambda]} \right)^{n'} \right. \\
&\cdot \left[(N-n)(N-n'-n+1) - \frac{1}{2}(N-n)(N-n+1) \right] I(N-n-n'-1) \\
&+ \sum_{n'=1}^{M_N} (N-n') W^{n'} (n'-1) + \sum_{n'=1}^{M_N} \left[\sum_{n=1+n'}^{M_N} \sum_{k=N-n'-n}^{N-n} \sum_{s=n-n'}^{N-n'-k} W^{s+n'} \right. \\
&\left. + \sum_{n=1+n'}^{M_N} \sum_{s=n-n'}^{n+1} (N-n'-n-1) W^{s+n'} \right] \\
&\left. + \sum_{n=1}^{M_N} (N-n) W^n \left[\frac{n^2}{2} + 2 - \frac{3}{2}n \right] \right\}
\end{aligned}$$

where

$$W = \frac{\beta e^{-\epsilon\alpha}}{\alpha + \beta}.$$

Proof: See appendix.

Lemma 3: If the process X is Gaussian and has a covariance function given by (4) then an asymptotic bound of $U_2(\lambda)$ as $N \rightarrow \infty$ is given by:

$$\begin{aligned}
U_2(\lambda) \leq Y_2(\lambda) &= \frac{A^2}{(\pi\beta)^2} \frac{M_N}{N} \left\{ \frac{1}{2} \operatorname{Rl} \left[(\alpha + \beta - i\lambda)^{-1} \left(\frac{2(\alpha + \beta)}{(\alpha + \beta)^2 + \lambda^2} \right) \right] \right. \\
&+ \frac{2}{M_N N} \sum_{n=1}^{M_N} \sum_{n'=1}^{M_N} \sum_{s=n}^{N-n'-1} (N-n'-s) W^{s+n'} I(N-n'-n-1) \\
&\left. + \operatorname{Rl} \left[\left[\frac{(\alpha + \beta - i\lambda)}{(\alpha + \beta - i\lambda) - \beta e^{-\epsilon(\alpha - i\lambda)}} \right] \left[\frac{2[(\alpha + \beta)^2 + \lambda^2] - \beta e^{-\epsilon\alpha} [2(\alpha + \beta) \cos(\epsilon\lambda) - 2\lambda \sin(\epsilon\lambda)]}{[(\alpha + \beta)^2 + \lambda^2] - \beta e^{-\epsilon\alpha} [2(\alpha + \beta) \cos(\epsilon\lambda) - 2\lambda \sin(\epsilon\lambda)] + \beta^2 e^{-2\epsilon\alpha}} \right] \right] \right\}
\end{aligned}$$

$$\begin{aligned}
& + \left[\frac{2(\alpha + \beta) - 2\beta e^{-\epsilon\alpha} \cos(\epsilon\alpha)}{[(\alpha + \beta)^2 + \lambda^2] - 2\beta e^{-\epsilon\alpha} [(\alpha + \beta) \cos(\epsilon\lambda) - \lambda \sin(\epsilon\lambda)] + \beta^2 e^{-2\epsilon\alpha}} \right] \\
& + \operatorname{Re} \left[\frac{\alpha + \beta - i\lambda}{(\alpha + \beta - i\lambda) - \beta e^{-\epsilon(\alpha - i\lambda)}} \right] \left[\frac{2(\alpha + \beta)}{(\alpha + \beta)^2 + \lambda^2} \right] + \operatorname{Re} \left[(\alpha + \beta - i\lambda)^{-1} \left(\frac{2(\alpha + \beta)}{(\alpha + \beta)^2 + \lambda^2} \right) \right] \\
& + 2 \operatorname{Re} \left[\frac{\alpha + \beta - i\lambda}{(\alpha + \beta - i\lambda) - \beta e^{-\epsilon(\alpha - i\lambda)}} \right]^2 \Bigg\} .
\end{aligned}$$

Proof: See appendix.

Lemma 4: If the process X is Gaussian and has covariance function (4) then an upper bound on $U_3(\lambda)$ is given by:

$$\begin{aligned}
U_3(\lambda) \leq Y_3(\lambda) &= \frac{2A^2}{(\pi\beta N)^2} \sum_{n=1}^{M_N} \left[\sum_{n'=1}^{M_N} \left(\frac{W^{N+1}}{(W-1)^2} (1 - W^{-N+n+n'}) - \frac{W^{n+n'}}{W-1} (N-n-n') \right) \right. \\
& + \sum_{n'=n}^{M_N} \sum_{k=N-n'-n+2}^{N-n} \frac{W}{W-1} (W^{N-k} - W^{n'}) + \sum_{n'=n}^{M_N} (N-n'-n+1) \frac{W^{n'}(W^{n'+n-1}-1)}{W^{n'}-1} \\
& \left. + W^n \left[3n^2N - 6nN + 6n^2 - \frac{7n^3}{3} - \frac{32n}{3} \right] + (N-n)W^{2n} + [4N-2]W^n \right] \\
& + \frac{2A^2}{(\pi\beta N)^2} \sum_{n'=1}^{M_N} \left[\sum_{n=n'}^{M_N} [N-n'-n+1] W^{n'} \frac{(W^{n'+n-1}-1)}{W^{n'}-1} \right. \\
& \left. + \sum_{n=n'}^{M_N} \sum_{k=N-n-n'+2}^{N-n} \frac{W}{W-1} (W^{N-k+1} - W^{n'}) + (N-n')(n'-1)W^{n'} \right] .
\end{aligned}$$

Note that $Y_3(\cdot)$ does not depend on λ .

Proof: See appendix.

Theorem 2: If X is a continuous parameter zero mean, fourth order, stationary, and Gaussian random process with covariance function given by (4), then an asymptotic bound on the variance of the estimator in (2) is given by

$$\begin{aligned} \text{Var} [\hat{\varphi}_N(\lambda)] &= U_1(\lambda) + U_2(\lambda) + U_3(\lambda) - E^2[\hat{\varphi}_N(\lambda)] \\ &\leq |Y_1(\lambda)| + |Y_2(\lambda)| + |Y_3(\lambda)| - |E^2[\hat{\varphi}_N(\lambda)]| \end{aligned} \quad (12)$$

as $N \rightarrow \infty$, $M_N \rightarrow \infty$, $M_N/N \rightarrow 0$.

Proof: The proof follows from Lemmata 2, 3, and 4.

The forms of $Y_1(\lambda)$, $Y_2(\lambda)$ and $Y_3(\lambda)$ are unfortunately very awkward and as a result, it is not easy to see how these equations behave. The summations in $Y_1(\lambda)$ and $Y_3(\lambda)$ may be eliminated through the long and tedious procedure of using geometric expansion type identities. This is presently being performed and when accomplished will greatly simplify the variance expression and provide an insight to the behavior of the variance. In addition, if the bounds $Y_1(\lambda)$ and $Y_3(\lambda)$ can be shown to be maximized at $\epsilon = 0$, then they can be bounded by the results in [1]:

$$U_1(\lambda) - E^2[\hat{\varphi}_N(\lambda)] = O(1/N)$$

$$U_3(\lambda) = O(1/N)$$

uniformly in λ as $N \rightarrow \infty$.

III. NUMERICAL AND SIMULATION RESULTS

Since the theoretical analysis, in Section II, showing the bias and variance of the time quantized spectral estimator, is somewhat involved and not easily interpreted, this section will provide insight into their behavior. Here we will present graphs of the bias as a function of frequency for several ϵ/β ratios, a numerical evaluation of the variance, and examples of time-quantized spectral estimates using simulated time series data.

Figure 2 is a graph of the spectral density for the process X where covariance function parameters α and A have been set equal to 1. This is representative of a nonbandlimited, low-pass spectrum. The peak of this spectrum is at $\lambda = 0$, the half power point at $\lambda = 1$, and the spectrum decreases at a rate proportional to $1/\lambda^2$. By adjusting the parameters α and A, the shape of the spectrum can be changed to broaden or narrow the peak. This spectral density will be used in the following numerical analysis of the bias and variance. The basic form of the covariance function C(t) used here which results from the solution of a first order homogeneous differential system can be combined [6] by addition to form the solution to a homogeneous differential system of arbitrary order.

BIAS:

Let the bias of the spectral estimator (2) be given by (6). We then define the percent bias as:

$$\% b[\hat{\varphi}_N(\lambda)] = \frac{b[\hat{\varphi}_N(\lambda)]}{\varphi(\lambda)}$$

Figures 3 through 8 are graphs of both the bias and percent bias as a function of frequency λ for several values of the average sampling rate β and time quantization ϵ . Three average sampling rates were used for the calculations of the bias. Figures 3 and 4 were generated with $\beta = 1$ rad/sec, Figures 5 and 6 were generated with $\beta = 5$ rad/sec and Figures 7 and 8 were generated

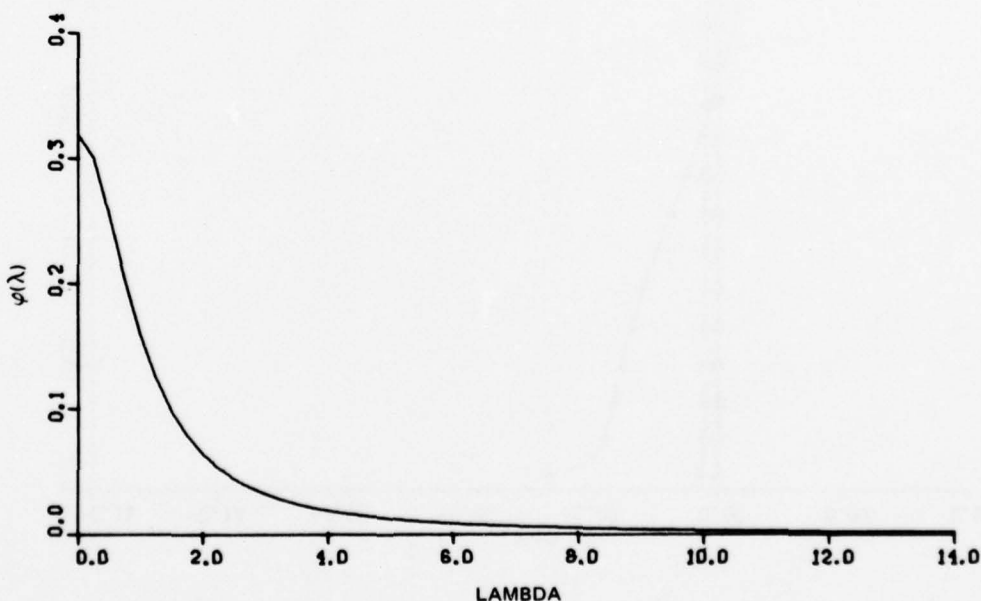


Figure 2. Spectral density function simulated for numerical analysis.

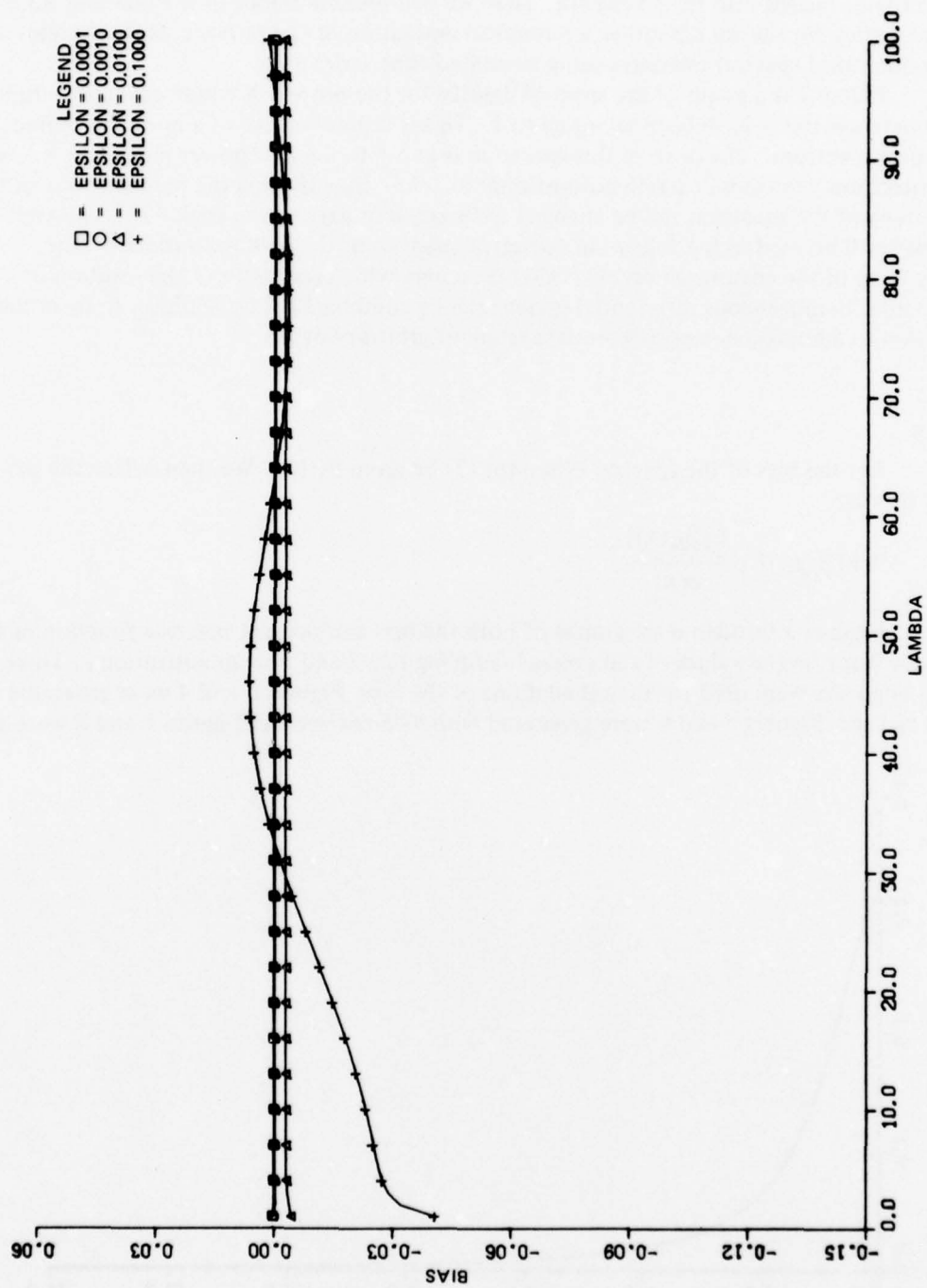


Figure 3. Bias of time-quantized Poisson spectral estimate as a function of frequency for $\beta = 1$ rad/sec, $N = 1000$ and $M_N = 7$.

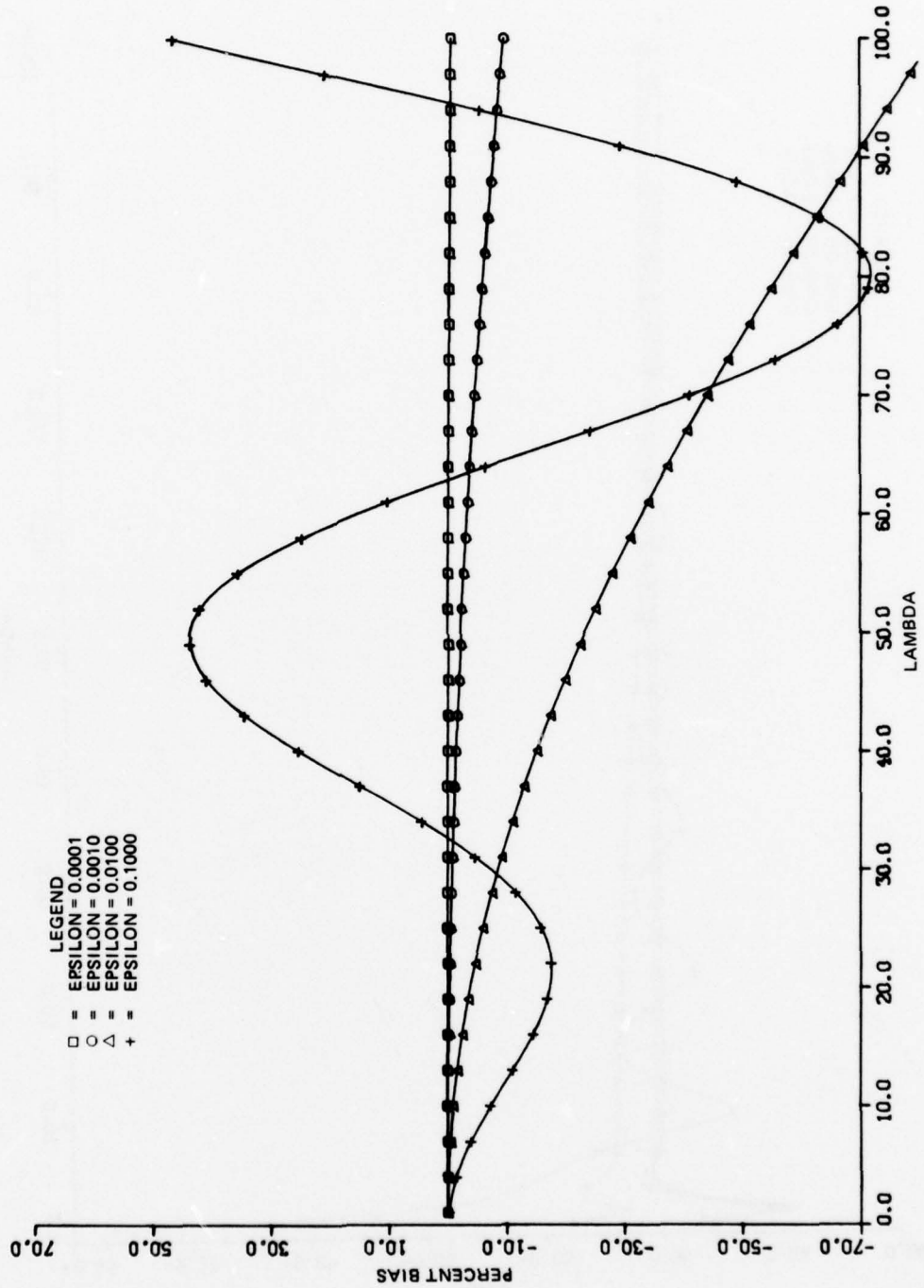


Figure 4. Percent bias of time-quantized Poisson spectral estimate as a function of frequency and epsilon for $\beta = 1$ rad/sec, $N = 1000$, and $M_N = 7$.

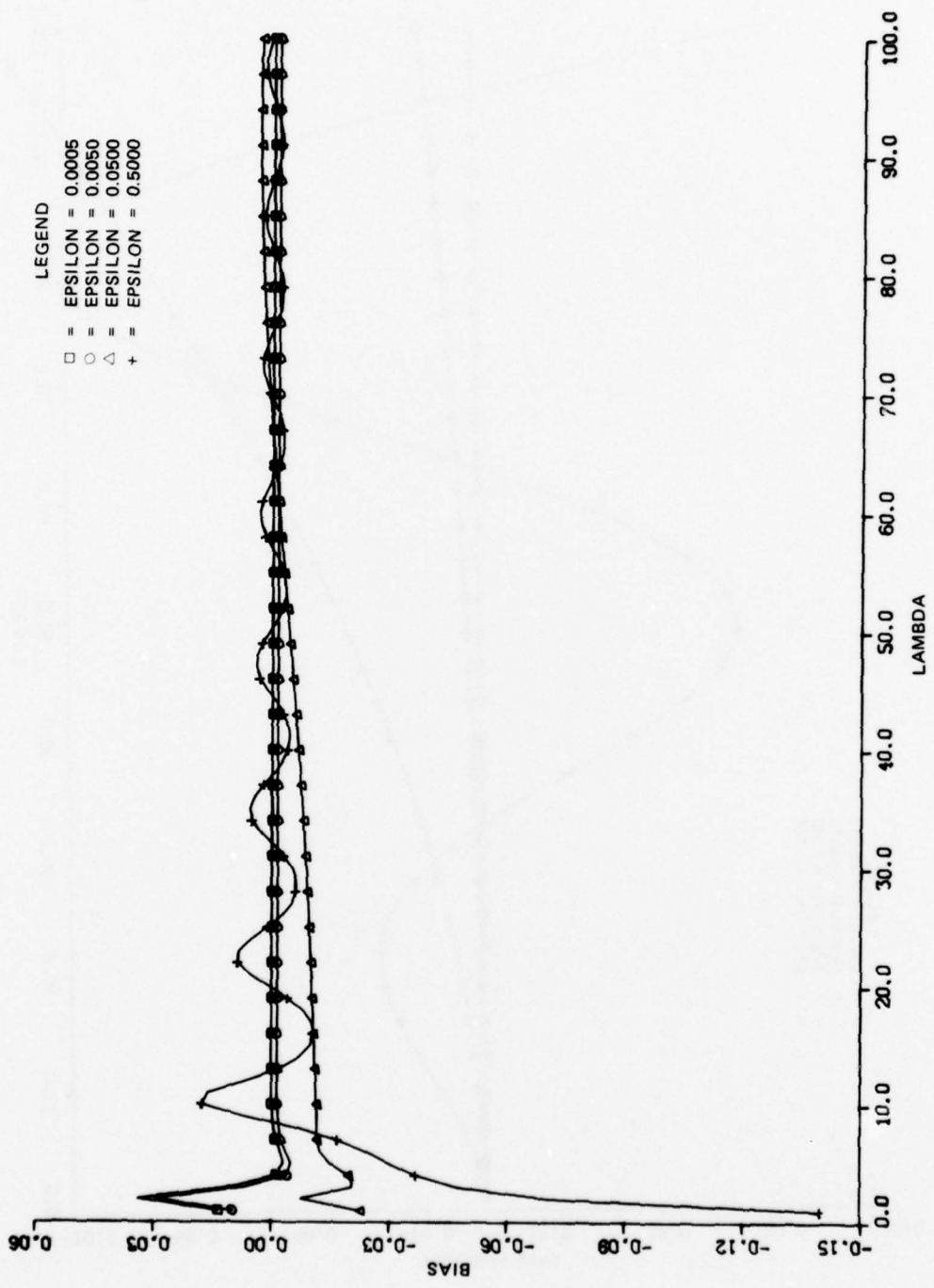


Figure 5. Bias of time-quantized Poisson spectral estimate as a function of frequency and epsilon for $\beta = 5$ rad/sec, $N = 1000$ and $M_N = 6$.

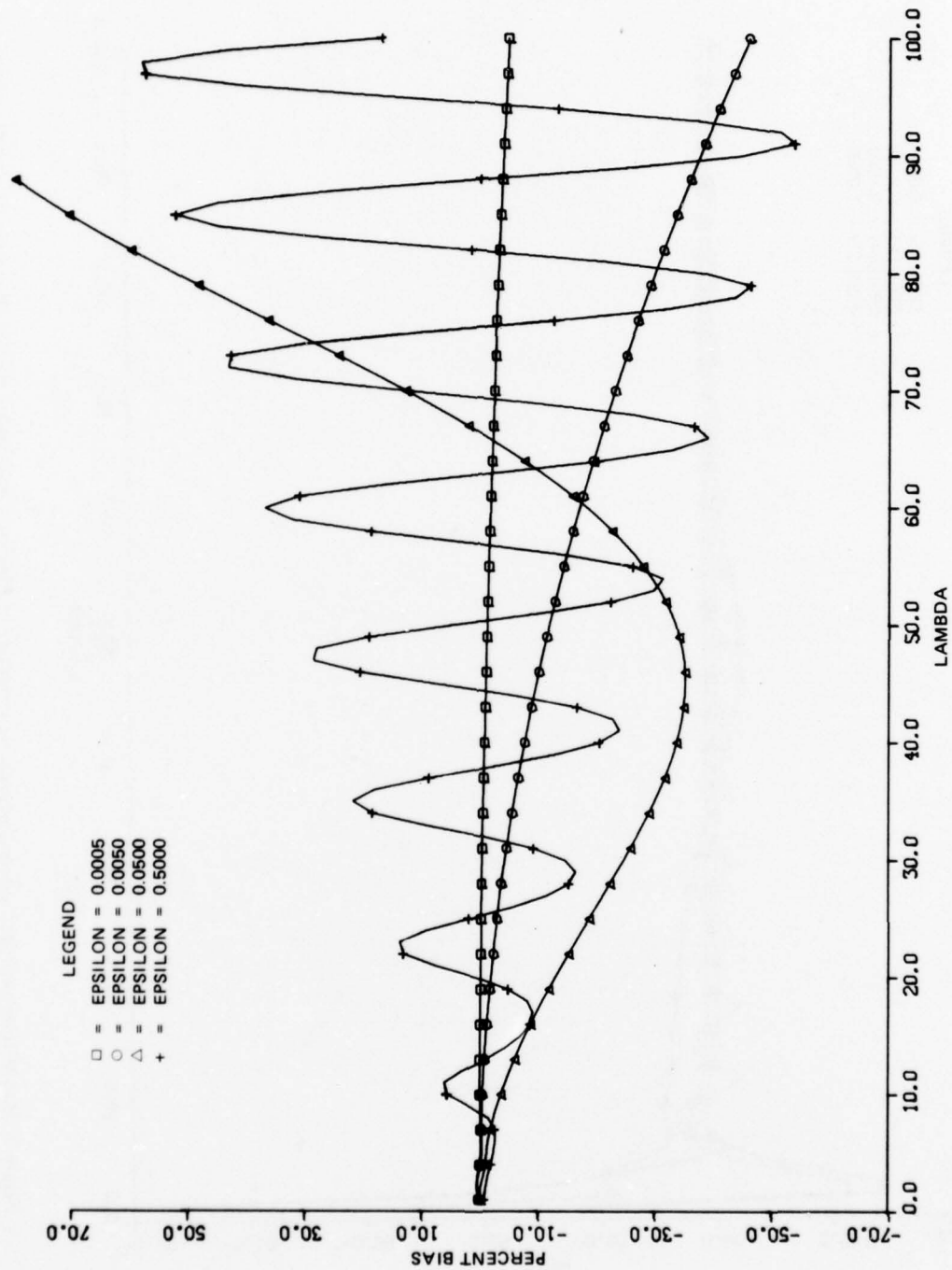


Figure 6. Percent bias of time-quantized spectral estimate as a function of frequency and epsilon for $\beta = 5$ rad/sec, $N = 1000$ and $M_N = 6$.

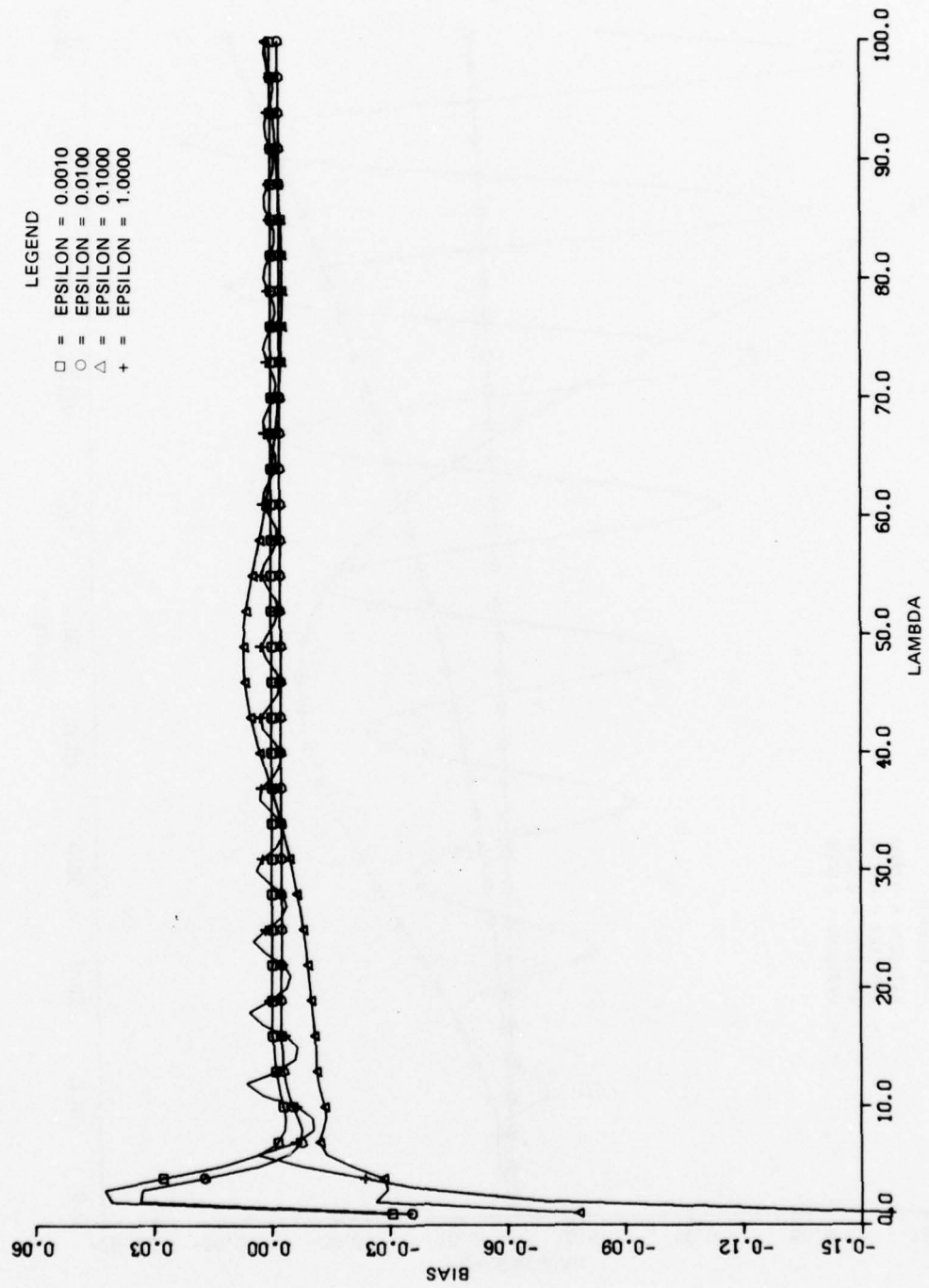


Figure 7. Bias of time-quantized spectral estimate as a function of frequency and epsilon for $\beta = 10$ rad/sec, $N = 1000$ and $M_N = 6$.

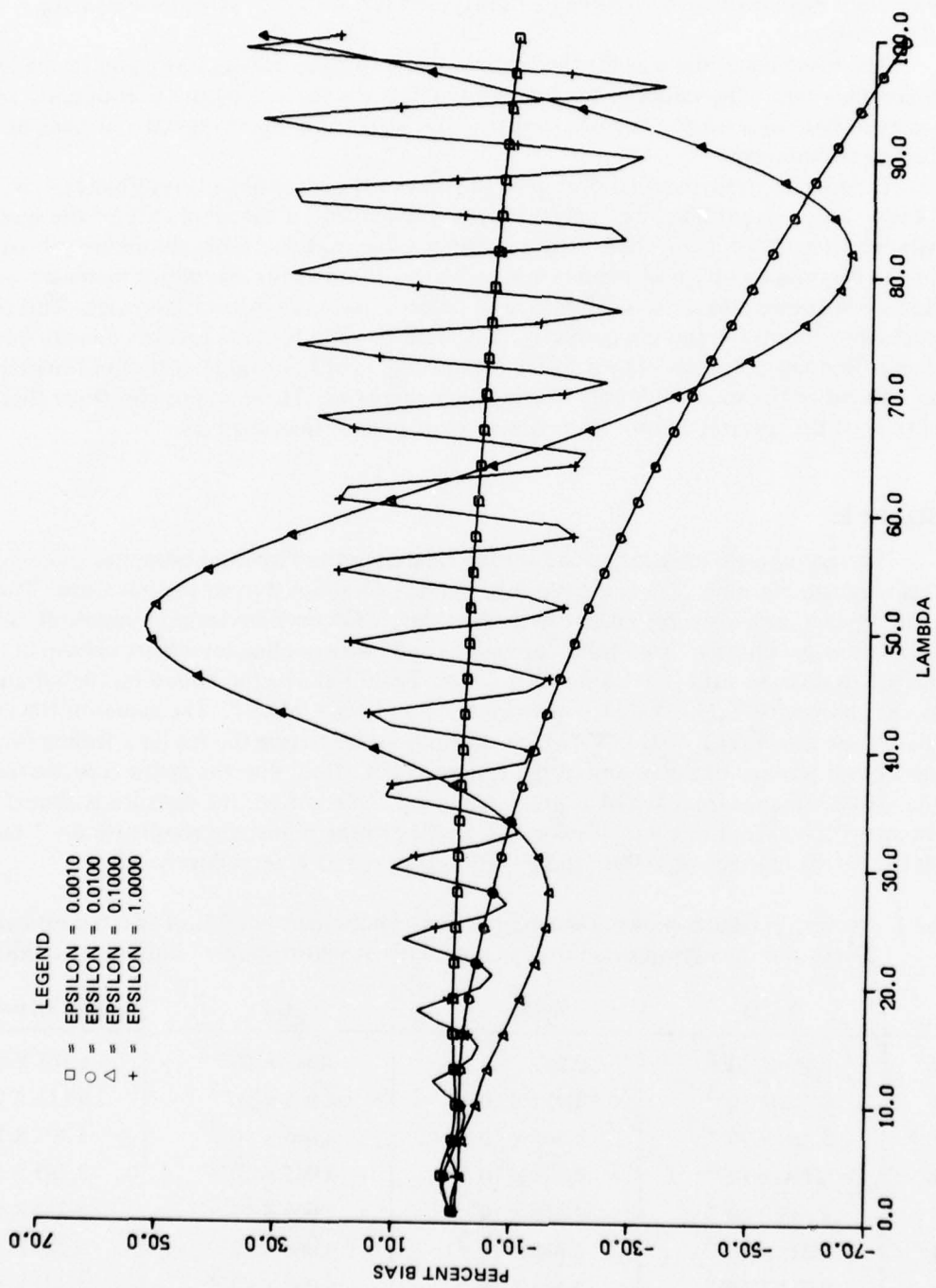


Figure 8. Percent bias of time-quantized spectral estimate as a function of frequency and epsilon for $\beta = 10$ rad/sec, $N = 1000$ and $M_N = 6$.

with $\beta = 10$ rad/sec. Each of the graphs contains 4 curves. These curves represent time quantization epsilons of 0.01, 0.1, 1.0 and 10.0 percent of the average sampling rate β . The horizontal axis of each graph represents frequency and the bias and percent bias are computed at frequency increments of 1. The value of M_N used is 6 for $\beta = 5, 10$ rad/sec and $M_N = 7$ for $\beta = 1$ rad/sec.

The behavior of the bias for the larger values of epsilon is oscillatory and increases with sampling rate. The values of the bias, although larger for $\lambda < 10$, are overall fairly small but as expected, increase as ϵ becomes larger. This is probably due to spectral aliasing of high frequency components.

In order to show the relationship of the bias to the spectral density, Figures 4, 6, and 8 represent percent bias. The percent bias is the percent of the amplitude of the spectral density which is offset due to bias. The parameter values in these three graphs are the same as for the bias graphs. Each of Figures 4, 6 and 8 shows a percent bias which increases with epsilon. The graphs also show a divergence of percent bias as frequency increases. This can be misleading unless interpreted correctly. It should be clear that the spectral density becomes smaller as frequency becomes larger which means that a constant value of bias becomes a larger percent of the spectral density as frequency increases. These graphs also show that the amplitude of the spectral density decreases at a rate greater than the bias.

VARIANCE

The asymptotic variance bound for the time-quantized spectral estimates given in (12) is very cumbersome. There is little that can be said about it in its present form. Therefore, in order to provide some insight to its behavior, it has been evaluated numerically for several sets of parameters. Two values of epsilon and two sampling rates were chosen in the numerical evaluation with $N = 1000$ and $M_N = 6$. Table 1 shows the bound on the variance of $\hat{\varphi}_N(\lambda)$ along with $Y_1(\lambda)$, $Y_2(\lambda)$, $Y_3(\lambda)$ for $\beta = 1$ and $\epsilon/\beta = 0.0001$. The values of the intermediary functions $Y_1(\lambda)$, $Y_2(\lambda)$, $Y_3(\lambda)$ are shown in order to give the reader a feeling for their relative contributions to the bound of the variance (12). Note that the major contribution to the variance comes from $Y_2(\lambda)$ as predicted in [1]. In addition, the variance is almost invariant with λ except at $\lambda = 0$. Tables 2, 3, and 4 provide numerical results for $\beta = 1$ rad/sec, $\epsilon = 0.01$; $\beta = 10$ rad/sec, $\epsilon = 0.001$; and $\beta = 10$ rad/sec, $\epsilon = 0.1$, respectively.

Table 1. Numerical results showing second moment component bounds of spectral estimator $\hat{\varphi}_N(\lambda)$ and the asymptotic variance bound of estimator for $\beta = 1$ rad/sec, $\epsilon = 0.0001$.

λ	$Y_1(\lambda)$	$Y_2(\lambda)$	$Y_3(\lambda)$	Var ($\hat{\varphi}_N(\lambda)$) bound
0	2.401×10^{-2}	0.243	4.065×10^{-3}	1.733×10^{-1}
10	5.313×10^{-4}	4.952×10^{-2}	4.065×10^{-3}	5.411×10^{-2}
20	5.326×10^{-4}	4.845×10^{-2}	4.065×10^{-3}	5.305×10^{-2}
30	5.331×10^{-4}	4.825×10^{-2}	4.065×10^{-3}	5.285×10^{-2}
40	5.333×10^{-4}	4.818×10^{-2}	4.065×10^{-3}	5.278×10^{-2}
50	5.333×10^{-4}	4.815×10^{-2}	4.065×10^{-3}	5.275×10^{-2}
60	5.333×10^{-4}	4.813×10^{-2}	4.065×10^{-3}	5.273×10^{-2}
70	5.333×10^{-4}	4.812×10^{-2}	4.065×10^{-3}	5.272×10^{-2}
80	5.332×10^{-4}	4.811×10^{-2}	4.065×10^{-3}	5.271×10^{-2}
90	5.331×10^{-4}	4.811×10^{-2}	4.065×10^{-3}	5.271×10^{-2}
100	5.330×10^{-4}	4.810×10^{-2}	4.065×10^{-3}	5.270×10^{-2}

Table 2. Numerical results showing second moment component bounds of spectral estimator $\hat{\varphi}_N(\lambda)$ and the asymptotic variance bound of estimator for $\beta = 1$ rad/sec, $\epsilon = 0.01$.

λ	$Y_1(\lambda)$	$Y_2(\lambda)$	$Y_3(\lambda)$	Var ($\hat{\varphi}_N(\lambda)$) bound
0	2.400×10^{-2}	0.239	3.942×10^{-3}	1.728×10^{-1}
10	5.313×10^{-4}	4.857×10^{-2}	3.942×10^{-3}	5.304×10^{-2}
20	5.326×10^{-4}	4.752×10^{-2}	3.942×10^{-3}	5.199×10^{-2}
30	5.331×10^{-4}	4.733×10^{-2}	3.942×10^{-3}	5.180×10^{-2}
40	5.333×10^{-4}	4.727×10^{-2}	3.942×10^{-3}	5.174×10^{-2}
50	5.333×10^{-4}	4.725×10^{-2}	3.942×10^{-3}	5.172×10^{-2}
60	5.333×10^{-4}	4.725×10^{-2}	3.942×10^{-3}	5.172×10^{-2}
70	5.333×10^{-4}	4.726×10^{-2}	3.942×10^{-3}	5.173×10^{-2}
80	5.332×10^{-4}	4.727×10^{-2}	3.942×10^{-3}	5.174×10^{-2}
90	5.331×10^{-4}	4.729×10^{-2}	3.942×10^{-3}	5.176×10^{-2}
100	5.329×10^{-4}	4.732×10^{-2}	3.942×10^{-3}	5.179×10^{-2}

Table 3. Numerical results showing second moment component bounds of spectral estimator $\hat{\varphi}_N(\lambda)$ and the asymptotic variance bound of estimator for $\beta = 10$ rad/sec, $\epsilon = 0.001$.

λ	$Y_1(\lambda)$	$Y_2(\lambda)$	$Y_3(\lambda)$	Var ($\hat{\varphi}_N(\lambda)$)
0	4.779×10^{-3}	5.741	7.626×10^{-4}	5.765
10	6.187×10^{-5}	3.553×10^{-2}	7.626×10^{-4}	4.506×10^{-2}
20	6.193×10^{-5}	4.435×10^{-2}	7.626×10^{-4}	4.467×10^{-2}
30	6.187×10^{-5}	4.598×10^{-2}	7.626×10^{-4}	4.680×10^{-2}
40	6.187×10^{-5}	4.654×10^{-2}	7.626×10^{-4}	4.736×10^{-2}
50	6.187×10^{-5}	4.680×10^{-2}	7.626×10^{-4}	4.762×10^{-2}
60	6.188×10^{-5}	4.693×10^{-2}	7.626×10^{-4}	4.775×10^{-2}
70	6.188×10^{-5}	4.702×10^{-2}	7.626×10^{-4}	4.784×10^{-2}
80	6.188×10^{-5}	4.707×10^{-2}	7.626×10^{-4}	4.789×10^{-2}
90	6.188×10^{-5}	4.711×10^{-2}	7.626×10^{-4}	4.793×10^{-2}
100	6.188×10^{-5}	4.714×10^{-2}	7.626×10^{-4}	4.796×10^{-2}

Table 4. Numerical results showing second moment component bounds of spectral estimator $\hat{\varphi}_N(\lambda)$ and the asymptotic variance bound of estimator for $\beta = 10$ rad/sec, $\epsilon = 0.1$.

λ	$Y_1(\lambda)$	$Y_2(\lambda)$	$Y_3(\lambda)$	$\text{Var}(\hat{\varphi}_N(\lambda))$
0	2.604×10^{-3}	1.550	3.403×10^{-4}	1.543
10	6.441×10^{-5}	2.109×10^{-2}	3.403×10^{-4}	2.139×10^{-2}
20	5.810×10^{-5}	2.509×10^{-2}	3.403×10^{-4}	2.541×10^{-2}
30	5.427×10^{-5}	3.344×10^{-2}	3.403×10^{-4}	3.381×10^{-2}
40	4.002×10^{-5}	5.624×10^{-2}	3.403×10^{-4}	5.661×10^{-2}
50	4.942×10^{-5}	7.090×10^{-2}	3.403×10^{-4}	7.124×10^{-2}
60	4.853×10^{-5}	5.252×10^{-2}	3.403×10^{-4}	5.291×10^{-2}
70	3.925×10^{-5}	4.113×10^{-2}	3.403×10^{-4}	4.150×10^{-2}
80	4.046×10^{-5}	3.890×10^{-2}	3.403×10^{-4}	3.927×10^{-2}
90	3.867×10^{-5}	4.276×10^{-2}	3.403×10^{-4}	4.314×10^{-2}
100	3.820×10^{-5}	5.130×10^{-2}	3.403×10^{-4}	5.168×10^{-2}

For the sake of illustration we generated time series data as in [2] for the spectral density of (5) with $A = \alpha = 1$, sampled it using several values of epsilon and, using the estimator (2), computed spectral estimates. The results are shown in Figures 9, 10, and 11 for $\beta = 1, 5,$ and 10 rad/sec, respectively. Here the epsilons used are the same as those used in computing the bias and percent bias. In these graphs the true spectral density $\varphi(\lambda)$ is represented by a solid curve without symbols. The vertical axis represents amplitude, while frequency is along the horizontal axis. Any negative estimates generated are set equal to zero since the spectral density by definition is everywhere positive. The number of data points used was $N = 1000$ and M_N was chosen by generating spectral estimates using several values of M_N and selecting the M_N which provided the best estimate (based on mean squared error).

In Figure 9 where the lowest average sampling rate was used ($\beta = 1$ rad/sec), the peak of the spectral density is generally estimated quite well. As the average sampling rate is increased (Figures 10 and 11), the values for the estimates of the peak become biased. This bias is predicted in Figures 3, 5, and 7 where bias near the origin increases both as a function of ϵ and as a function of β . It also appears in Figures 9, 10, and 11 that spectral estimates for $\lambda > 5$ improve with increasing the value of β . There is no periodic type structure in any of the estimates that would suggest spectral aliasing as one might expect, especially for the larger epsilons.

Spectral estimates for the case when $\epsilon = 0$ were computed and observed to be almost identical for the case $\epsilon/\beta = 0.01\%$. For this reason, spectral estimates for $\epsilon = 0$ are not shown on the graphs.

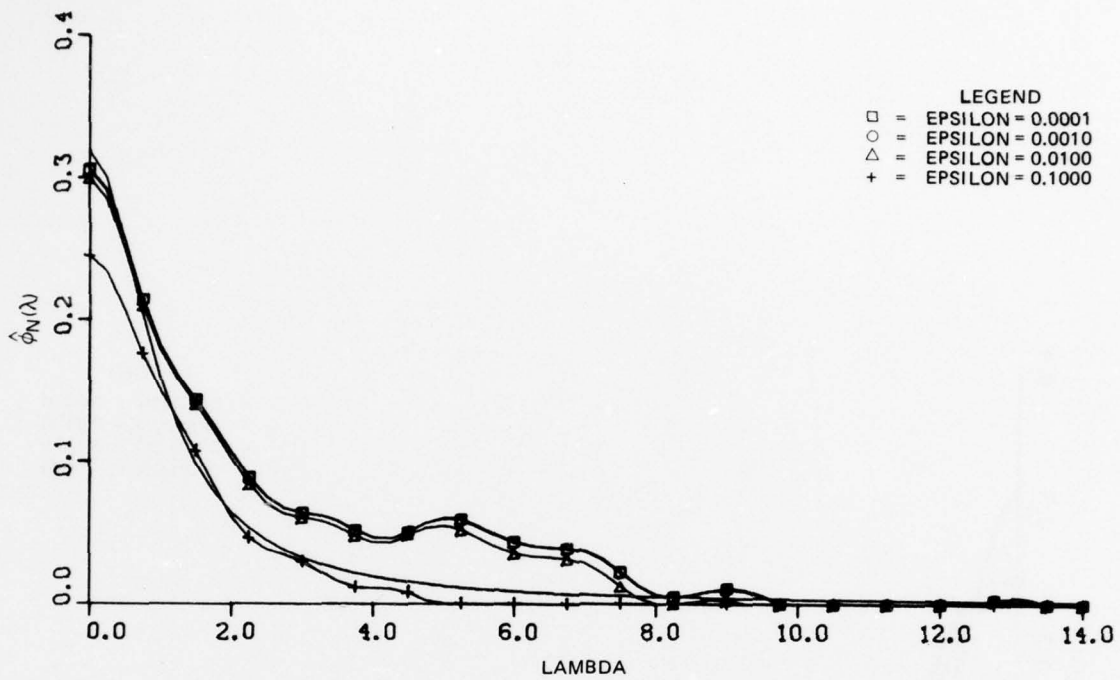


Figure 9. Spectral estimate for $\beta = 1$ rad/sec, $M_N = 7$ and several values of epsilon.

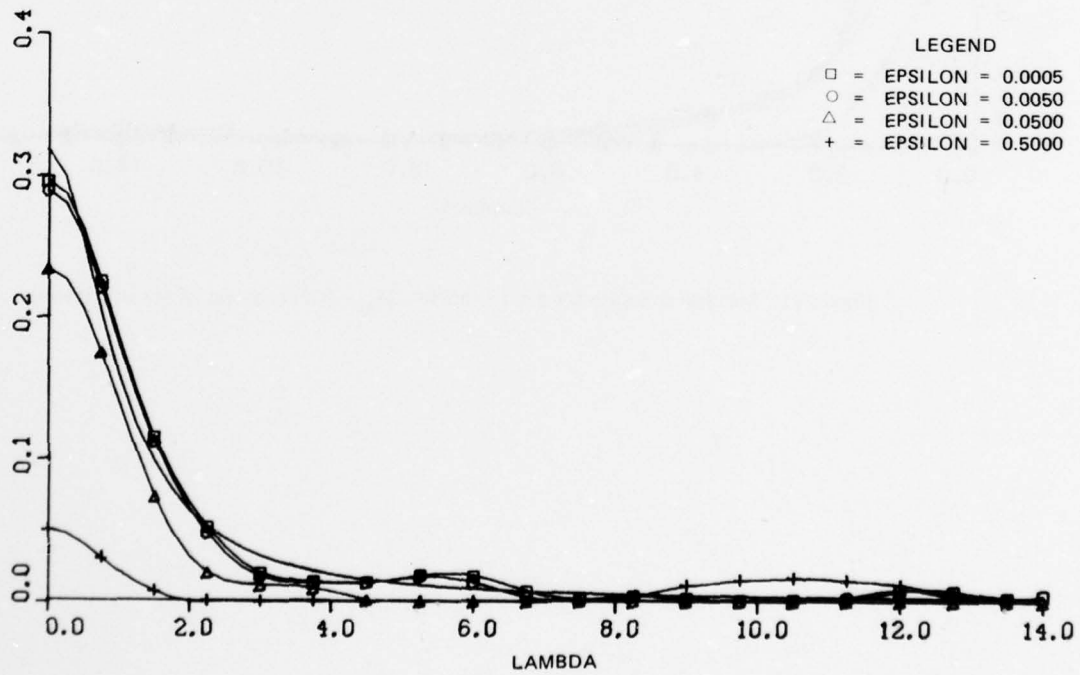


Figure 10. Spectral estimate for $\beta = 5$ rad/sec, $M_N = 6$ and several values of epsilon.

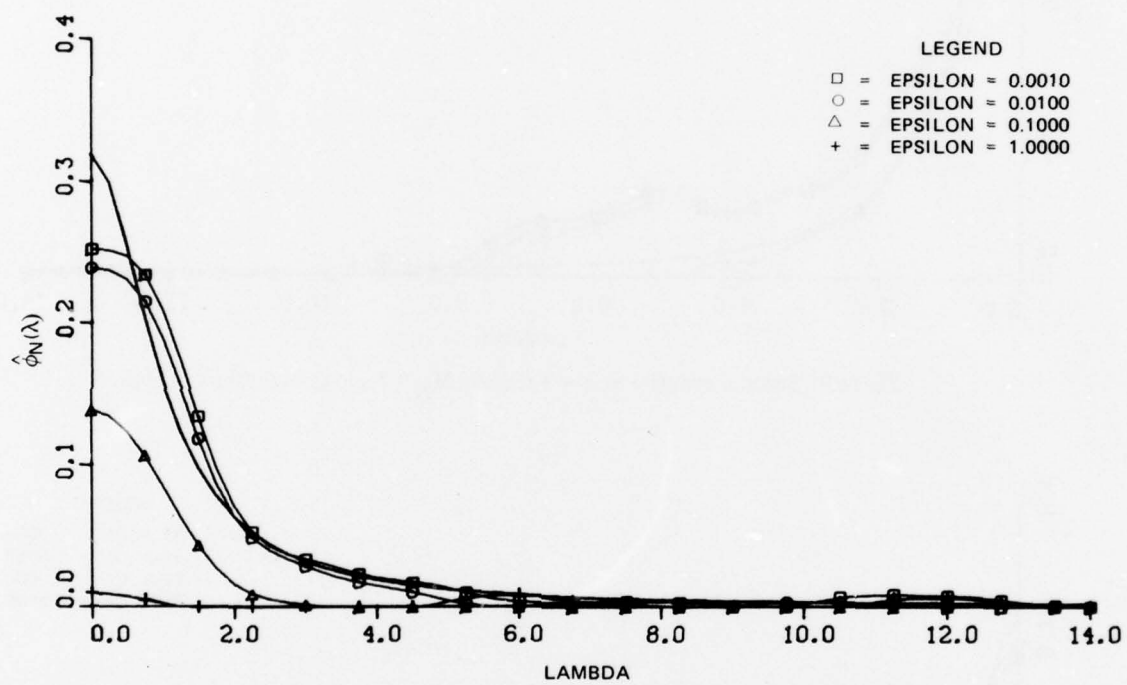


Figure 11. Spectral estimate for $\beta \approx 10$ rad/sec, $M_N = 6$ and several values of epsilon.

IV. CONCLUSIONS

This report has shown results of an examination of the spectral estimator proposed in [1] for time-quantized Poisson distributed sampling intervals. The probability density function for the time-quantized Poisson samples as well as the bias and a bound for the variance of the spectral estimator for a large class of spectra have been derived.

On performing a numerical analysis, the bias of the spectral estimator was seen to increase with increasing average sample rate β and decrease with frequency λ at a rate between λ and λ^2 . In all cases examined the bias appeared to be largest in the region around $\lambda = 0$ and increased with epsilon.

The bound for the variance of the spectral estimator, which was derived through a complicated procedure, resulted in a cumbersome asymptotic expression. With useful information difficult to extract from this bound, it was evaluated numerically and found to be small with respect to the spectral density except near the origin. In addition, except near the origin, it was found to have small dependence on the value of the average sampling rate.

It was shown, using synthetically-generated data, that the behavior of the time quantized spectral estimator was similar to that predicted by the theoretical bias particularly near the origin and not adverse to that of the variance bound. This simulation also showed that degradation of the spectral estimates was small for ϵ/β ratios of less than 0.1%, but for larger ϵ/β ratios the effect was quite pronounced. The measure of degradation used was integrated mean squared error over the range of the graphs. It is not clear if mean squared error is the best measure of degradation since other measures were available, but it was used in order to be consistent with [2]. Another measure of degradation which could be used is the quality of estimates of the peak of the spectrum. For this measure the results are the same; larger epsilon yields more degradation.

The results in this report indicate that for the class of spectral densities examined, a time quantization of the Poisson sample point of up to 0.1% of the average sampling rate may perhaps be tolerated.

There are several questions which remain unanswered concerning this time quantized Poisson sampling problem and should be pursued. First of all, the asymptotic bound for the variance of the estimator should be simplified and a determination of its tightness be made. It is not clear that for $\epsilon = 0$ the bias and variance results reported here are bounded by or equal to the results of [1]. This should be determined. The effects of using different covariance weighting functions should be examined for the time quantized case. Finally, other more complicated spectral densities, such as a narrowband signal modulated by a carrier signal, could be examined for results comparable to those reported here.

V. APPENDIX

Here we present proofs of Lemmata 2, 3, and 4 which, when combined, make up a bound for the second moment of the spectral estimator (2) for the Gaussian case, with zero mean.

As was previously mentioned in section II, the expectation with respect to t_n in (8) cannot be evaluated unless it is examined over regions involving the different permutations of $\{k, k', k+n, k'+n'\}$. These nonintersecting regions R_i are defined in [1] and are:

$$\begin{aligned}
 R_1 &= (k < k+n \leq k' < k'+n' \mid k, k' \in \mathbb{R}) \\
 R_2 &= (k < k' < k+n < k'+n' \mid k, k' \in \mathbb{R}) \\
 R_3 &= (k = k' < k+n < k'+n' \mid k, k' \in \mathbb{R}) \\
 R_4 &= (k < k' < k+n = k'+n' \mid k, k' \in \mathbb{R}) \\
 R_5 &= (k = k' < k+n = k'+n' \mid k, k' \in \mathbb{R}) \\
 R_6 &= (k < k' < k'+n' < k+n \mid k, k' \in \mathbb{R}) \\
 R_7 &= (k = k' < k'+n' < k+n \mid k, k' \in \mathbb{R}) \\
 R_8 &= (k' < k'+n' \leq k < k+n \mid k, k' \in \mathbb{R}) \\
 R_9 &= (k' < k < k'+n' < k+n \mid k, k' \in \mathbb{R}) \\
 R_{10} &= (k' < k < k'+n' = k+n \mid k, k' \in \mathbb{R}) \\
 R_{11} &= (k' < k < k+n < k'+n' \mid k, k' \in \mathbb{R})
 \end{aligned} \tag{A-1}$$

The union of these regions is equivalent to summing over the indices k and k' of (8) or

$$R = \bigcup_{i=1}^{11} R_i.$$

There is considerable symmetry between pairs of the regions defined in (A-1) which can be used in evaluating (9), (10), and (11). Let $U_k(\lambda)$, $k = 1, 2, 3$ be the sum of $U_k^i(\lambda)$ over the regions R_i , specifically:

$$U_k(\lambda) = \sum_{i=1}^{11} U_k^i(\lambda). \tag{A-2}$$

Then by the symmetry of the regions:

$$\begin{aligned}
 U_k^1(\lambda) &= U_k^8 \\
 U_k^2(\lambda) &= U_k^9(\lambda) \\
 U_k^3(\lambda) &= U_k^7(\lambda)
 \end{aligned}$$

$$U_k^4(\lambda) = U_k^{10}(\lambda)$$

$$U_k^6(\lambda) = U_k^{11}(\lambda)$$

and we can write (A-2) as

$$U_k(\lambda) = U_k^5(\lambda) + 2 \sum_{\substack{i=1 \\ i \neq 5}}^6 U_k^i(\lambda). \quad (\text{A-3})$$

In order to prove Lemma 3 we will need the following relationships which are shown in [1].

Let

$$\{b_n\}_{n=0}^{\infty}$$

and

$$\{c_n\}_{n=0}^{\infty}$$

be two sequences of complex numbers which are absolutely summable and let d be a complex number such that $0 < |d| \leq 1$. We then define

$$Q_i = \frac{1}{N^2} \sum_{n=1}^{M_N} \sum_{n'=1}^{M_N} \sum_{(k,k' \in R_i)}^{N-n} \sum_{N-n'}^{N-n'} b_{k'-k} d^{n-(k'-k)} C_{k'-k+n'-n} \quad (\text{A-4})$$

$i = 2, \dots, 5$

$$Q_6 = \frac{1}{N^2} \sum_{n=1}^{M_N} \sum_{n'=1}^{M_N} \sum_{(k,k' \in R_6)}^{N-n} \sum_{N-n'}^{N-n'} b_{k'-k} d^{n'} C_{n-n'+k'-k}. \quad (\text{A-5})$$

As $N \rightarrow \infty$ we have the following asymptotic behavior:

$$Q_2 = \begin{cases} O(1/N) & |d| < 1 \\ \frac{M_N}{N} \left[\sum_{r=1}^{\infty} b_r \right] \left[\sum_{s=1}^{\infty} C_s \right] & d = 1 \end{cases} \quad (\text{A-6})$$

$$Q_3 = \begin{cases} O(1/N) & |d| < 1 \\ \frac{M_N}{N} b_0 \left[\sum_{s=1}^{\infty} C_s \right] & d = 1 \end{cases} \quad (\text{A-7})$$

$$Q_4 = \begin{cases} O(1/N) & |d| < 1 \\ \frac{M_N}{N} C_0 \left[\sum_{r=1}^{\infty} b_r \right] & d = 1 \end{cases} \quad (\text{A-8})$$

$$Q_5 = \begin{cases} O(1/N) & |d| < 1 \\ b_0 C_0 \frac{M_N}{N} & d = 1 \end{cases} \quad (\text{A-9})$$

$$Q_6 = \begin{cases} O(1/N) & |d| < 1 \\ \frac{M_N}{N} \left[\sum_{r=1}^{\infty} b_r \right] \left[\sum_{s=1}^{\infty} C_s \right] & d = 1. \end{cases} \quad (\text{A-10})$$

Proof of Lemma 2:

We have from (A-3)

$$U_1(\lambda) = U_1^5(\lambda) + 2 \sum_{\substack{i=1 \\ i \neq 5}}^6 U_1^i(\lambda)$$

where

$$U_1^i(\lambda) = \frac{1}{(\pi N \beta)^2} \sum_{n=1}^{M_N} \sum_{n'=1}^{M_N} \sum_{k, k' \in R_i}^{N-n} \sum_{N-n'}^{N-n'} E_{t_n} [C(t_{k+n} - t_k) C(t_{k'+n'} - t_{k'})] \cdot \cos [\lambda(t_{k+n} - t_k)] \cos [\lambda(t_{k'+n'} - t_{k'})]. \quad (\text{A-11})$$

In the sequel, $U_1^i(\lambda)$ will be considered separately for each region R_i and we will use the notation $f_n(t)$ as a shortened version of $f_{t_n}(t)$.

Region R_1 :

Since the intervals $t_{k+n} - t_k$ and $t_{k'+n'} - t_{k'}$ are stationary and independent then we can write:

$$U_1^1(\lambda) = \frac{1}{(\pi N \beta)^2} \sum_{n=1}^{M_N} \sum_{n'=1}^{M_N} z_n z_{n'} \sum_{k, k' \in R_1}^{N-n} \sum_{N-n'}^{N-n'} \quad (\text{A-12})$$

where

$$z_n = \int_0^{\infty} C(t) \cos(\lambda t) f_n(t) dt.$$

Evaluating the double sum over (k, k') in the region R_1 we have

$$U_1^1(\lambda) = \frac{1}{(\pi N \beta)^2} \sum_{n=1}^{M_N} \sum_{n'=1}^{M_N} z_n z_{n'} \left[(N-n)(N-n'-n+1) - \frac{1}{2} (N-n)(N-n+1) I(N-n-n'-1) \right] \quad (\text{A-13})$$

where $I(\cdot)$ is the indicator function, i.e.,

$$I(N-n-n'-1) = 1 \quad \text{if } N-n-n'-1 \geq 0$$

$$I(N-n-n'-1) = 0, \quad \text{otherwise.}$$

As an example of evaluating multiple sums over regions we will go through the steps in evaluating the double sum in (A-12) over R_1 .

$$\begin{aligned} \sum_{k,k' \in R_1}^{N-n} \sum_{k'=1}^{N-n'} 1 &= \sum_{k=1}^{N-n} \sum_{k'=1}^{N-n'} I(k < k+n \leq k' < k'+n') \\ &= \sum_{k=1}^{N-n} \sum_{k'=1}^N I(k' \leq N-n') I(1 \leq n) I(n \leq k'-k) I(1 \leq n'). \end{aligned}$$

Now let $s = k' - k$ and we have

$$\begin{aligned} \sum_{k=1}^{N-n} \sum_{s=1}^N I(s \leq N-n'-k) I(1 \leq n) I(n \leq s) I(1 \leq n') \\ = \sum_{k=1}^{N-n-n} \sum_{s=n}^{N-n'-k} 1 = \sum_{k=1}^{N-n} N-n'-n+1-k \\ = (N-n)(N-n'-n+1) - \frac{1}{2}(N-n)(N-n+1). \end{aligned}$$

Now we solve the integrals z_n and $z_{n'}$ using Lemma 1 and (4).

$$\begin{aligned} z_n &= \int_0^{\infty} C(t) \cos(\lambda t) f_n(t) dt \\ &= A \int_0^{\infty} e^{-\alpha|t|} \cos(\lambda t) \beta^n \frac{(t-\epsilon n)^{n-1}}{(n-1)!} e^{-\beta(t-\epsilon n)} U(t-\epsilon n) dt \\ &= \frac{A\beta^n e^{\beta\epsilon n}}{2(n-1)!} \left\{ \int_{\epsilon n}^{\infty} e^{-t[(\alpha+\beta)-i\lambda]} (t-\epsilon n)^{n-1} + e^{-t[(\alpha+\beta)+i\lambda]} (t-\epsilon n)^{n-1} dt \right\} \\ &= \frac{A\beta^n e^{\beta\epsilon n}}{2(n-1)!} \left\{ [(\alpha+\beta)-i\lambda]^{-n} e^{-\epsilon n[(\alpha+\beta)-i\lambda]} \Gamma(n) \right. \\ &\quad \left. + [(\alpha+\beta)+i\lambda]^{-n} e^{-\epsilon n[(\alpha+\beta)+i\lambda]} \Gamma(n) \right\} \end{aligned}$$

$$\begin{aligned}
&= \frac{A\beta^n}{2} \left[\left(\frac{e^{-\epsilon[\alpha - i\lambda]}}{[(\alpha + \beta) - i\lambda]} \right)^n + \left(\frac{e^{-\epsilon[\alpha + i\lambda]}}{[(\alpha + \beta) + i\lambda]} \right)^n \right] \\
&= \frac{A\beta^n}{2} \operatorname{Rl} \left(\frac{e^{-\epsilon[\alpha - i\lambda]}}{[(\alpha + \beta) - i\lambda]} \right)^n
\end{aligned} \tag{A-14}$$

Similarly we have for $z_{n'}$:

$$z_{n'} = \frac{A\beta^{n'}}{2} \operatorname{Rl} \left(\frac{e^{-\epsilon[\alpha - i\lambda]}}{[(\alpha + \beta) - i\lambda]} \right)^{n'} \tag{A-15}$$

Now using (A-14) and (A-15) in (A-13) we have

$$\begin{aligned}
U_1^1(\lambda) &= \frac{A^2}{4(\pi N\beta)^2} \sum_{n=1}^{M_N} \sum_{n'=1}^{M_N} \beta^{n+n'} \operatorname{Rl} \left(\frac{e^{-\epsilon[\alpha - i\lambda]}}{[(\alpha + \beta) - i\lambda]} \right)^n \operatorname{Rl} \left(\frac{e^{-\epsilon[\alpha - i\lambda]}}{[(\alpha + \beta) - i\lambda]} \right)^{n'} \\
&\quad \cdot \left[(N-n)(N-n'-n+1) - \frac{1}{2}(N-n)(N-n+1) \right] I(N-n-n'-1).
\end{aligned}$$

In each of the regions 2-6 we have a dependence between $\{C(t_{k+n} - t_k) \cos \lambda(t_{k+n} - t_k)\}$ and $\{C(t_{k'+n'} - t_{k'}) \cos \lambda(t_{k'+n'} - t_{k'})\}$ which makes the expectation in (A-11) very difficult to solve. We will deal with this dependency by choosing appropriate bounds for the intervals $(t_{k+n} - t_k)$ and $(t_{k'+n'} - t_{k'})$ which will make them independent. The bounds selected [1] are as follows.

If $\gamma \triangleq t_{k+n} - t_k$, then we have

$$\gamma \geq \begin{cases} t_{k'} - t_k & i = 2 \\ t_{k+n} - t_k & i = 3 \\ t_{k'} - t_k & i = 4 \\ t_{k+n} - t_k & i = 5 \\ (t_{k'} - t_k) + (t_{k+n} - t_{k'+n'}) & i = 6 \end{cases}$$

and if $\delta \triangleq t_{k'+n'} - t_{k'}$ then

$$\delta \geq \begin{cases} t_{k'+n'} - t_{k+n} & i = 2 \\ t_{k'+n'} - t_{k+n} & i = 3 \\ t_{k'+n'} - t_{k'} & i = 4 \\ t_{k'+n'} - t_{k'} & i = 5 \\ t_{k'+n'} - t_{k'} & i = 6. \end{cases}$$

We also will use the bound

$$|C(\tau) \cos \lambda\tau| \leq |C(\tau)|$$

in evaluating (A-11) for these regions.

Using these bounds we have the following:

$$U_1^2(\lambda) \leq \frac{1}{(\pi\beta N)^2} \sum_{n=1}^{M_N} \sum_{n'=1}^{M_N} \sum_{R, k'}^{N-n} \sum_{\epsilon R_2}^{N-n'} \int_0^\infty |C(t)| f_{k'-k}(t) dt \int_0^\infty |C(\tau)| f_{n'}(\tau) d\tau \quad (\text{A-16})$$

$$U_1^3(\lambda) \leq \frac{1}{(\pi\beta N)^2} \sum_{n=1}^{M_N} \sum_{n'=1}^{M_N} \sum_{k, k'}^{N-n} \sum_{\epsilon R_3}^{N-n'} \int_0^\infty |C(t)| f_n(t) dt \int_0^\infty |C(\tau)| f_{n'-n}(\tau) d\tau$$

$$U_1^4(\lambda) \leq \frac{1}{(\pi\beta N)^2} \sum_{n=1}^{M_N} \sum_{n'=1}^{M_N} \sum_{k, k'}^{N-n} \sum_{\epsilon R_4}^{N-n'} \int_0^\infty |C(t)| f_{k'-k}(t) dt \int_0^\infty |C(\tau)| f_{n'}(\tau) d\tau$$

$$U_1^5(\lambda) \leq \frac{1}{(\pi\beta N)^2} \sum_{n=1}^{M_N} \sum_{n'=1}^{M_N} \sum_{k, k'}^{N-n} \sum_{\epsilon R_5}^{N-n'} \left[\int_0^\infty |C(t)| f_n(t) dt \right]^2$$

$$U_1^6(\lambda) \leq \frac{1}{(\pi\beta N)^2} \sum_{n=1}^{M_N} \sum_{n'=1}^{M_N} \sum_{k, k'}^{N-n} \sum_{\epsilon R_6}^{N-n'} \int_0^\infty |C(t)| f_{n-n'}(t) dt \int_0^\infty |C(\tau)| f_{n'}(\tau) d\tau$$

Region R-2

From (A-16), Lemma 1 and (5) we have

$$\begin{aligned} U_1^2(\lambda) &\leq \frac{A^2}{(\pi\beta N)^2} \sum_{n=1}^{M_N} \sum_{n'=1}^{M_N} \sum_{k, k'}^{N-n} \sum_{\epsilon R_2}^{N-n'} \frac{\beta^{k'-k}}{(k'-k-1)!} e^{\beta\epsilon(k'-k)} \int_{\epsilon(k'-k)}^\infty e^{-t(\alpha+\beta)} [t-\epsilon(k'-k)]^{k'-k-1} dt \\ &\quad \cdot \frac{\beta^{n'}}{(n'-1)!} e^{\beta\epsilon n'} \int_{\epsilon n'}^\infty e^{-t(\alpha+\beta)} (t-\epsilon n')^{n'-1} dt \\ &= \frac{A^2}{(\pi\beta N)^2} \sum_{n=1}^{M_N} \sum_{n'=1}^{M_N} \sum_{k, k'}^{N-n} \sum_{\epsilon R_2}^{N-n'} \frac{W^{k'-k}}{(k'-k-1)!} e^{-\epsilon(\alpha+\beta)(k'-k)} \Gamma(k'-k) \\ &\quad \cdot \frac{\beta^{n'}}{(n'-n)!} \frac{e^{\beta\epsilon n'}}{\alpha+\beta} e^{-\epsilon n'(\alpha+\beta)} \Gamma(n') \\ &= \frac{A^2}{(\pi\beta N)^2} \sum_{n=1}^{M_N} \sum_{n'=1}^{M_N} \sum_{k, k'}^{N-n} \sum_{\epsilon R_2}^{N-n'} W^{k'-k+n'} \end{aligned}$$

Now let $s = k' - k$ and we have

$$= \frac{A^2}{(\pi\beta N)^2} \sum_{n=1}^{M_N} \sum_{n'=1}^{M_N} \sum_{k=1}^{N-n} \sum_{s=1}^{N-n'-k} W^{s+n'} I(s \leq n-1) I(n-n' < s) I(s \geq 1).$$

Consider the four situations:

(1) $n - n' < 1$ and $N - n' - k \leq n - 1$

$$\frac{A^2}{(\pi\beta N)^2} \sum_{n=1}^{M_N} \sum_{n'=1}^{M_N} \sum_{k=N-n'-n+1}^{N-n} \sum_{s=1}^{N-n'-k} W^{s+n'} I(n - n' < 1) I(N - n' - k \leq n - 1) \quad (\text{A-17})$$

(2) $n - n' < 1$ and $N - n' - k > n - 1$

$$\frac{A^2}{(\pi\beta N)^2} \sum_{n=1}^{M_N} \sum_{n'=1}^{M_N} \sum_{k=1}^{N-n'-n} \sum_{s=1}^{n-1} W^{s+n'} I(n - n' < 1) I(n - 1 < N - n' - k) \quad (\text{A-18})$$

(3) $n - n' \geq 1$ and $N - n' - k \leq n - 1$

$$\frac{A^2}{(\pi\beta N)^2} \sum_{n=1}^{M_N} \sum_{n'=1}^{M_N} \sum_{k=N-n'-n+1}^{N-n} \sum_{s=n-n'}^{N-n'-k} W^{s+n'} I(n - n' \geq 1) I(N - n' - k \leq n - 1) \quad (\text{A-19})$$

(4) $n - n' \geq 1$ and $N - n' - k > n - 1$

$$\frac{A^2}{(\pi\beta N)^2} \sum_{n=1}^{M_N} \sum_{n'=1}^{M_N} \sum_{k=1}^{N-n'-n} \sum_{s=n-n'}^{n-1} W^{s+n'} I(n - n' \geq 1) I(n - 1 < N - n' - k). \quad (\text{A-20})$$

Summing expressions (A-17), (A-18), (A-19), and (A-20) and simplifying we have:

$$\begin{aligned} U_1^2(\lambda) \leq & \frac{A^2}{(\pi\beta N)^2} \sum_{n'=1}^{M_N} \left\{ \sum_{n=1}^{n'} \sum_{k=N-n'-n+1}^{N-n} \sum_{s=1}^{N-n'-k} W^{s+n'} \right. \\ & + \sum_{n=1}^{n'} \sum_{s=1}^{n-1} (N - n' - n) W^{s+n'} + \sum_{n=n'+1}^{M_N} \sum_{k=N-n'-n+1}^{N-n} \sum_{s=n-n'}^{N-n'-k} W^{s+n'} \\ & \left. + \sum_{n=n'+1}^{M_N} \sum_{s=n-n'}^{n-1} (N - n' - n) W^{s+n'} \right\} \end{aligned}$$

The procedure for evaluating $U_1(\lambda)$ over regions R-3 through R-6 is very similar to its evaluation over R-2. Therefore, we only state the results.

Region R-3

$$U_1^3(\lambda) \leq \frac{A^2}{(\pi\beta N)^2} \sum_{n'=1}^{M_N} (N - n') W^{n'(n'-1)}$$

Region R-4

$$U_1^4(\lambda) \leq \frac{A^2}{(\pi\beta N)^2} \sum_{n'=1}^{M_N} \left\{ \sum_{n=1+n'}^{M_N} \sum_{k=N-n'-n}^{N-n} \sum_{s=n-n'}^{N-n'-k} W^{s+n'} \right. \\ \left. + \sum_{n=1+n'}^{M_N} \sum_{s=n-n'}^{n+1} (N - n' - n - 1) W^{s+n'} \right\}$$

Region R-5

$$U_1^5(\lambda) \leq \frac{A^2}{(\pi\beta N)^2} \sum_{n=1}^{M_N} (N - n) W^{2n}$$

Region R-6

$$U_1^6(\lambda) \leq \frac{A^2}{(\pi\beta N)^2} \sum_{n=1}^{M_N} (N - n) W^n \left[\frac{n^2}{2} + 2 - \frac{3}{2}n \right].$$

Finally, using (A-3) and the results for each region we have:

$$U_1(\lambda) \leq \frac{A^2}{(\pi\beta N)^2} \sum_{n=1}^{M_N} (N - n) W^{2n} \\ + \frac{2A^2}{(\pi\beta N)^2} \left\{ \frac{1}{4} \sum_{n=1}^{M_N} \sum_{n'=1}^{M_N} \beta^{n+n'} \operatorname{Re} \left(\frac{e^{-\epsilon[\alpha-i\lambda]}}{[(\alpha+\beta)-i\lambda]} \right)^n \operatorname{Re} \left(\frac{e^{-\epsilon[\alpha-i\lambda]}}{[(\alpha+\beta)-i\lambda]} \right)^{n'} \left[(N-n)(N-n'-n+1) \right. \right. \\ \left. \left. - \frac{1}{2} (N-n)(N-n+1) \right] \cdot I(N-n-n'-1) + \sum_{n'=1}^{M_N} (N - n') W^{n'(n'-1)} \right\}$$

$$\begin{aligned}
& + \sum_{n'=1}^{M_N} \left[\sum_{n=1+n'}^{M_N} \sum_{k=N-n'-n}^{N-n} \sum_{s=n-n'}^{N-n'-k} W^{s+n'} + \sum_{n=1+n'}^{M_N} \sum_{s=n-n'}^{n+1} (N-n'-n-1) W^{s+n'} \right] \\
& + \sum_{n=1}^{M_N} (N-n) W^n \left[\frac{n^2}{2} + 2 - \frac{3}{2}n \right] \}
\end{aligned}$$

Proof of Lemma 3:

As in the proof of Lemma 2 we will use (A-3) and consider each region separately.

Region R-1

We begin here using (10) and noting that:

$$\begin{aligned}
U_2^1(\lambda) & \leq |U_2^1(\lambda)| \\
& \leq \frac{1}{(\pi\beta N)^2} \sum_{n=1}^{M_N} \sum_{n'=1}^{M_N} \sum_{k,k' \in R_1}^{N-n} \sum_{N-n'}^{N-n'} E_{t_n} |C(t_{k'} - t_k) C(t_{k+n} - t_{k'+n'})|
\end{aligned}$$

and using the bound $t_{k'} - t_k \geq t_{k+n} - t_{k'+n'}$, which is independent of $t_{k+n} - t_{k'+n'}$, we have:

$$\leq \frac{1}{(\pi\beta N)^2} \sum_{n=1}^{M_N} \sum_{n'=1}^{M_N} \sum_{k,k' \in R_1}^{N-n} \sum_{N-n'}^{N-n'} E_{t_n} |C(t_{k+n} - t_k)| E_{t_n} |C(t_{k+n} - t_{k'+n'})|.$$

Substituting for $f_n(t)$, the value of $C(t)$ and performing the integration results in:

$$U_2^1(\lambda) \leq \frac{A^2}{(\pi\beta N)^2} \sum_{n=1}^{M_N} \sum_{n'=1}^{M_N} \sum_{k,k' \in R_1}^{N-n} \sum_{N-n'}^{N-n'} W^{k'+n'-k} \quad \text{when } W = \frac{\beta e^{\epsilon\alpha}}{\alpha + \beta}.$$

Now letting $s = k' - k$ and simplifying we have

$$U_2^1(\lambda) \leq \frac{A^2}{(\pi\beta N)^2} \sum_{n=1}^{M_N} \sum_{n'=1}^{M_N} \sum_{s=n}^{N-n'-1} (N-n'-s) W^{s+n'} I(N-n'-n-1)$$

Next we consider regions R-2 through R-5 and beginning with (10) we have:

$$\begin{aligned}
U_2^i(\lambda) & = \sum_{n=1}^{M_N} \sum_{n'=1}^{M_N} \sum_{k,k' \in R_i}^{N-n} \sum_{N-n'}^{N-n'} E_t C(t_{k'} - t_k) C(t_{k+n} - t_{k'+n'}) \\
& \quad \cdot \cos [\lambda(t_{k+n} - t_k)] \cos [\lambda(t_{k'+n'} - t_{k'})].
\end{aligned} \tag{A-21}$$

Using the substitutions: $\theta = t_{k'} - t_k$, $\eta = t_{k+n} - t_k$, $\Delta = t_{k'+n'} - t_{k'}$ yields

$$= \sum_{n=1}^{M_N} \sum_{n'=1}^{M_N} \sum_{k,k' \in R_i} \sum_{N-n}^{N-n'} \iiint C(\theta) C(\Delta) \cos [\lambda(\theta + \eta)] \cos [\lambda(\eta + \Delta)] \quad (A-22)$$

$$\cdot f_{k'-k}(\theta) f_{n-k'+k}(\eta) f_{n'-n+k'-k}(\Delta) d\theta d\eta d\Delta.$$

Expressing the cosines as exponentials, regrouping terms, and using (1) we can express (A-22) as:

$$= \frac{A^2}{2(\pi\beta N)^2} \sum_{n=1}^{M_N} \sum_{n'=1}^{M_N} \sum_{k,k' \in R_i} \sum_{N-n}^{N-n'} \text{Re} \left\{ \int_0^\infty e^{-\theta(\alpha-i\lambda)} f_{k'-k}(\theta) d\theta \left[\int_0^\infty e^{-\Delta(\alpha-i\lambda)} f_{n'-n+k'-k}(\Delta) d\Delta \right. \right.$$

$$\left. \left. \cdot \varphi^{n-k'+k}(2\lambda) + \int_0^\infty e^{-\Delta(\alpha+i\lambda)} f_{n'-n+k'-k}(\Delta) d\Delta \varphi^{n-k'+k}(0) \right] \right\}. \quad (A-23)$$

This is the same form as (A-4) which will enable us to use (A-6) through (A-9) and hence determine the asymptotic behavior of $U_2^1(\lambda)$.

Region R-2

Using (A-6) we can express (A-23) for region R-2 as:

$$\frac{A^2}{2(\pi\beta)^2} \frac{M_N}{N} \text{Re} \left\{ \left[\sum_{r=1}^{\infty} \int_0^\infty e^{-\theta(\alpha-i\lambda)} f_{k'-k}(\theta) d\theta \right] \left[\sum_{s=1}^{\infty} \int_0^\infty e^{-\Delta(\alpha-i\lambda)} f_{n'-n+k'-k}(\Delta) d\Delta \right] \right.$$

$$\left. + \left[\sum_{r=1}^{\infty} \int_0^\infty e^{-\theta(\alpha-i\lambda)} f_{k'-k}(\theta) d\theta \right] \left[\sum_{s=1}^{\infty} \int_0^\infty e^{-\Delta(\alpha+i\lambda)} f_{n'-n+k'-k}(\Delta) d\Delta \right] \right\}. \quad (A-24)$$

Now, by using Lemma 1, evaluating the integrals, and then simplifying, we have for (A-24)

$$\frac{A^2}{2(\pi\beta)^2} \frac{M_N}{N} \text{Re} \left\{ \sum_{r=1}^{\infty} \left(\frac{\beta}{\alpha+\beta-i\lambda} \right)^r e^{-r\epsilon(\alpha-i\lambda)} \sum_{s=1}^{\infty} \left(\frac{\beta}{\alpha+\beta-i\lambda} \right)^s e^{-s\epsilon(\alpha-i\lambda)} \right.$$

$$\left. + \sum_{r=1}^{\infty} \left(\frac{\beta}{\alpha+\beta-i\lambda} \right)^r e^{-r\epsilon(\alpha-i\lambda)} \sum_{s=1}^{\infty} \left(\frac{\beta}{\alpha+\beta+i\lambda} \right)^s e^{-s\epsilon(\alpha+i\lambda)} \right\}. \quad (A-25)$$

Finally, summing (A-25) and rearranging terms yields

$$U_2^2(\lambda) = \frac{A^2}{(\pi\beta)^2} \frac{M_N}{2N} \operatorname{Re} \left\{ \left[\frac{(\alpha + \beta - i\lambda)}{(\alpha + \beta - i\lambda) - \beta e^{-\epsilon(\alpha - i\lambda)}} \right] \cdot \left[\frac{2[(\alpha + \beta)^2 + \lambda^2] - \beta e^{-\epsilon\alpha} [2(\alpha + \beta) \cos(\epsilon\lambda) - 2\lambda \sin(\epsilon\lambda)]}{[(\alpha + \beta)^2 + \lambda^2] - \beta e^{-\epsilon\alpha} [2(\alpha + \beta) \cos(\epsilon\lambda) - 2\lambda \sin(\epsilon\lambda)] + \beta^2 e^{-2\epsilon\alpha}} \right] \right\}$$

as $N \rightarrow \infty$.

Equation (A-23) is solved in a very similar manner in regions R-3, R-4, and R-5 and here we will only state the results.

Region R-3

$$U_2^3(\lambda) = \frac{A^2}{2(\pi\beta)^2} \frac{M_N}{N} \left[\frac{2(\alpha + \beta) - 2\beta e^{-\epsilon\alpha} \cos(\epsilon\alpha)}{[(\alpha + \beta)^2 + \lambda^2] - 2\beta e^{-\epsilon\alpha} [(\alpha + \beta) \cos(\epsilon\lambda) - \lambda \sin(\epsilon\lambda)] + \beta^2 e^{-2\epsilon\alpha}} \right]$$

$N \rightarrow \infty$.

Region R-4

$$U_2^4(\lambda) = \frac{A^2}{2(\pi\beta)^2} \frac{M_N}{N} \operatorname{Re} \left\{ \left[\frac{\alpha + \beta - i\lambda}{(\alpha + \beta - i\lambda) - \beta e^{-\epsilon(\alpha - i\lambda)}} \right] \left[\frac{2(\alpha + \beta)}{(\alpha + \beta)^2 + \lambda^2} \right] \right\}$$

$N \rightarrow \infty$

Region R-5

$$U_2^5(\lambda) = \frac{A^2}{2(\pi\beta)^2} \frac{M_N}{N} \operatorname{Re} \left\{ (\alpha + \beta - i\lambda)^{-1} \left[\frac{2(\alpha + \beta)}{(\alpha + \beta)^2 + \lambda^2} \right] \right\}$$

$N \rightarrow \infty$.

For region R-6 we use the substitutions: $\theta = t_{k'} - t_k$, $\eta = t_{k'+n'} - t_{k'}$ and $\Delta = t_{k+n} - t_{k'+n'}$ in equation (A-21) which gives us:

$$U_2^6(\lambda) = \frac{A^2}{2(\pi\beta N)^2} \sum_{n=1}^{M_N} \sum_{n'=1}^{M_N} \sum_{k,k'}^{N-n} \sum_{\epsilon \in R_6}^{N-n'} \iiint C(\theta) C(\Delta) \cos(\lambda\eta) \cos(\lambda(\Delta + \eta + \theta)) \cdot f_{k'-k}(\theta) f_{k'+n'-k'}(\eta) f_{k+n-k'-n'}(\Delta) d\theta d\Delta d\eta.$$

Again, as in (A-22) we express the cosines as exponentials and regroup which yields

$$U_2^6(\lambda) = \frac{1}{2(\pi\beta N)^2} \sum_{k=1}^{M_N} \sum_{k'=1}^{M_N} \sum_{k,k'}^{N-n} \sum_{\epsilon \in R_6}^{N-n'} \operatorname{Re} \left\{ \int C(\theta) e^{i\lambda\theta} f_{k'-k}(\theta) d\theta \right. \quad (A-26)$$

$$\begin{aligned} & \cdot \int C(\Delta) e^{i\lambda\Delta} f_{k+n-k'-n'}(\Delta) d\Delta [\varphi(2\lambda)]^{n'} + \int C(\theta) e^{-i\lambda\theta} f_{k'-k}(\theta) d\theta \quad (\text{A-26}) \\ & \cdot \int C(\Delta) e^{-i\lambda\Delta} f_{k+n-k'-n'}(\Delta) d\Delta \left. \right\}. \end{aligned}$$

We note that (A-26) is of the same form as (A-5), thus using (A-10) we have

$$\begin{aligned} U_2^6(\lambda) &= \frac{1}{2(\pi\beta)^2} \frac{M_N}{N} \text{Rl} \left\{ \sum_{r=1}^{\infty} \int C(\theta) e^{i\lambda\theta} f_r(\theta) d\theta \sum_{s=1}^{\infty} \int C(\Delta) e^{i\lambda\Delta} f_s(\Delta) d\Delta \right. \\ & \quad \left. + \sum_{r=1}^{\infty} \int C(\theta) e^{-i\lambda\theta} f_r(\theta) d\theta \sum_{s=1}^{\infty} \int C(\Delta) e^{-i\lambda\Delta} f_s(\Delta) d\Delta \right\}. \end{aligned}$$

Using Lemma 1, solving the integrals and simplifying yields

$$U_2^6(\lambda) = \frac{A^2}{(\pi\beta)^2} \frac{M_N}{N} \text{Rl} \left[\frac{(\alpha+\beta-i\lambda)}{(\alpha+\beta-i\lambda) - \beta e^{-\epsilon(\alpha-i\lambda)}} \right]^2$$

$N \rightarrow \infty$.

Finally, using (A-3) we have the asymptotic result

$$\begin{aligned} U_2(\lambda) &\leq \frac{A^2}{(\pi\beta)^2} \frac{M_N}{N} \left\{ \frac{1}{2} \text{Rl} \left[(\alpha+\beta-i\lambda)^{-1} \left(\frac{2(\alpha+\beta)}{(\alpha+\beta)^2 + \lambda^2} \right) \right] \right. \\ & \quad \left. + \frac{2}{M_N N} \sum_{n=1}^{M_N} \sum_{n'=1}^{M_N} \sum_{s=n}^{N-n'-1} (N-n'-s) W^{s+n'} I(N-n'-n-1) \right. \\ & \quad \left. + \text{Rl} \left\{ \left[\frac{(\alpha+\beta-i\lambda)}{(\alpha+\beta-i\lambda) - \beta e^{-\epsilon(\alpha-i\lambda)}} \right] \left[\frac{2\{(\alpha+\beta)^2 + \lambda^2\} - \beta e^{-\epsilon\alpha} [2(\alpha+\beta) \cos(\epsilon\lambda) - 2\lambda \sin(\epsilon\lambda)]}{[(\alpha+\beta)^2 + \lambda^2] - \beta e^{-\epsilon\alpha} [2(\alpha+\beta) \cos(\epsilon\lambda) - 2\lambda \sin(\epsilon\lambda)] + \beta^2 e^{-2\epsilon\alpha}} \right] \right\} \right. \\ & \quad \left. + \left[\frac{2(\alpha+\beta) - 2\beta e^{-\epsilon\alpha} \cos(\epsilon\alpha)}{[(\alpha+\beta)^2 + \lambda^2] - 2\beta e^{-\epsilon\alpha} [(\alpha+\beta) \cos(\epsilon\lambda) - \lambda \sin(\epsilon\lambda)] + \beta^2 e^{-2\epsilon\alpha}} \right] \right. \\ & \quad \left. + \text{Rl} \left[\frac{(\alpha+\beta-i\lambda)}{(\alpha+\beta-i\lambda) - \beta e^{-\epsilon(\alpha-i\lambda)}} \right] \left[\frac{2(\alpha+\beta)}{(\alpha+\beta)^2 + \lambda^2} \right] + \text{Rl} \left[(\alpha+\beta-i\lambda)^{-1} \left(\frac{2(\alpha+\beta)}{(\alpha+\beta)^2 + \lambda^2} \right) \right] \right. \\ & \quad \left. + 2 \text{Rl} \left[\frac{(\alpha+\beta-i\lambda)}{(\alpha+\beta-i\lambda) - \beta e^{-\epsilon(\alpha-i\lambda)}} \right]^2 \right\} \end{aligned}$$

as $N \rightarrow \infty$.

Proof of Lemma 4:

The proof of this Lemma is similar to that of Lemma 2. From (11) we have

$$U_3(\lambda) = \frac{1}{(\pi\beta N)^2} \sum_{n=1}^{M_N} \sum_{n'=1}^{M_N} \sum_{k=1}^{N-n} \sum_{k'=1}^{N-n'} E_{t_n} \left\{ C(t_{k'+n'} - t_k) C(t_{k'} - t_{k+n}) \right. \\ \left. \cdot \cos [\lambda(t_{k+n} - t_k)] \cos [\lambda(t_{k'+n'} - t_{k'})] \right\}.$$

As before we will use (A-3) and consider the regions R-1 through R-6. Following the procedure used in the proof of Lemma 2 we define bounds on $(t_{k'+n'} - t_k)$ and $(t_{k'} - t_{k+n})$ which will make them independent in each of the six regions considered. We have from [1], the following sets of bounds.

For $\delta \triangleq t_{k'+n'} - t_k$ we use the bounds

$$\delta \geq \begin{cases} (t_{k+n} - t_k) + (t_{k'+n'} - t_{k'}) & i = 1 \\ (t_{k'} - t_k) + (t_{k'+n'} - t_{k+n}) & i = 2 \\ (t_{k'+n'} - t_{k+n}) & i = 3 \\ t_{k'+n'} - t_{k'} & i = 4 \\ t_{k'+n'} - t_k & i = 5 \\ t_{k'} - t_k & i = 6 \end{cases}$$

and for $\gamma \triangleq t_{k'} - t_{k+n}$ we simply use $(t_{k'} - t_{k+n})$ for all six regions.

Using these bounds and (A-3) we have the following expressions

$$U_3(\lambda) \leq \frac{1}{(\pi\beta N)^2} \sum_{n=1}^{M_N} \sum_{n'=1}^{M_N} \sum_{k,k' \in R_5} \int C(\tau) f_n(\tau) d\tau \int C(\tau) f_{n'}(\tau) d\tau \quad (A-27) \\ + \frac{2}{(\pi\beta N)^2} \sum_{n=1}^{M_N} \sum_{n'=1}^{M_N} \sum_{k,k' \in R_1} \int C(\tau) f_{k'-k-n}(\tau) d\tau \int C(\tau) f_{n+n'}(\tau) d\tau \\ + \frac{2}{(\pi\beta N)^2} \sum_{n=1}^{M_N} \sum_{n'=1}^{M_N} \sum_{k,k' \in R_2} \int C(\tau) f_{n+k-k'}(\tau) d\tau \int C(\tau) f_{2(k'-k)+n'-n}(\tau) d\tau \\ + \frac{2}{(\pi\beta N)^2} \sum_{n=1}^{M_N} \sum_{n'=1}^{M_N} \sum_{k,k' \in R_3} \int C(\tau) f_n(\tau) d\tau \int C(\tau) f_{n'-n}(\tau) d\tau \\ + \frac{2}{(\pi\beta N)^2} \sum_{n=1}^{M_N} \sum_{n'=1}^{M_N} \sum_{k,k' \in R_4} \int C(\tau) f_{n'}(\tau) d\tau \int C(\tau) f_{n-n'}(\tau) d\tau$$

$$+ \frac{2}{(\pi\beta N)^2} \sum_{n=1}^{M_N} \sum_{n'=1}^{M_N} \sum_{k, k' \in R_6} \int C(\tau) f_{n+k-k'}(\tau) d\tau \int C(\tau) f_{k'-k}(\tau) d\tau. \quad (\text{A-27})$$

To solve the integrals and evaluate (A-27) one follows the same procedure as in the proof of Lemma 2. Since this procedure is quite lengthy we will state the results for each of the six regions.

Region R-1

$$U_3^1(\lambda) \leq \frac{A^2}{(\pi\beta N)^2} \sum_{n=1}^{M_N} \sum_{n'=1}^{M_N} \sum_{k=1}^{N-n} \sum_{s=n}^{N-n'-k} W^{s+n}. \quad (\text{A-28})$$

Region R-2

$$\begin{aligned} U_3^2(\lambda) \leq & \frac{A^2}{(\pi\beta N)^2} \left\{ \sum_{n=1}^{M_N} \sum_{n'=n}^{M_N} \sum_{k=N-n'-n+2}^{N-n} \sum_{s=1}^{N-n'-k} W^{s+n'} \right. \\ & + \sum_{n=1}^{M_N} \sum_{n'=n}^{M_N} \sum_{s=1}^{n-1} (N-n'-n+1) W^{s+n'} + \sum_{n'=1}^{M_N} \sum_{n=n'+1}^{M_N} \sum_{s=1}^{n-1} (N-n'-n+1) W^{s+n'} \\ & \left. + \sum_{n'=1}^{M_N} \sum_{n=n'+1}^{M_N} \sum_{k=N-n'-n+2}^{N-n} \sum_{s=1}^{N-n'-k+1} W^{s+n'} \right\} \quad (\text{A-29}) \end{aligned}$$

Region R-3

$$U_3^3(\lambda) \leq \frac{A^2}{(\pi\beta N)^2} \sum_{n'=1}^{M_N} (N-n') (n'-1) W^{n'} \quad (\text{A-30})$$

Region R-4

$$U_3^4(\lambda) \leq \frac{A^2}{(\pi\beta N)^2} \sum_{n=1}^{M_N} W^n \left\{ 2n^2 N - 3nN + 3n^2 - \frac{4n^3}{3} - \frac{32n}{3} \right\} \quad (\text{A-31})$$

Region R-5

$$U_3^5(\lambda) \leq \frac{A^2}{(\pi\beta N)^2} \sum_{n=1}^{M_N} (N-n) W^{2n} \quad (A-32)$$

Region R-6

$$U_3^6(\lambda) \leq \frac{A^2}{(\pi\beta N)^2} \sum_{n=1}^{M_N} W^n \{N(4+n(n-3)) + n(n(3-n)-2)\} \quad (A-33)$$

Now, using (A-3) and (A-28) to (A-33) and simplifying we can express the bound for $U_3(\lambda)$ as:

$$\begin{aligned} U_3(\lambda) \leq & \frac{2A^2}{(\pi\beta N)^2} \sum_{n=1}^{M_N} \left[\sum_{n'=1}^{M_N} \left(\frac{W^{N+1}}{(W-1)^2} (1 - W^{-N+n+n'}) - \frac{W^{n+n'}}{W-1} (N-n-n') \right) \right. \\ & + \sum_{n'=n}^{M_N} \sum_{k=N-n'-n+2}^{N-n} \frac{W}{W-1} (W^{N-k} - W^{n'}) + \sum_{n'=n}^{M_N} (N-n'-n+1) \frac{W^{n'}(W^{n'+n-1} - 1)}{W^{n'} - 1} \\ & \left. + W^n \left[3n^2N - 6nN + 6n^2 - \frac{7n^3}{3} - \frac{32n}{3} \right] + (N-n) W^{2n} + W^n [4N-2] \right] \\ & + \frac{2A^2}{(\pi\beta N)^2} \sum_{n'=1}^{M_N} \left[\sum_{n=n'}^{M_N} [N-n'-n+1] W^{n'} \frac{(W^{n'+n-1} - 1)}{W^{n'} - 1} \right. \\ & \left. + \sum_{n=n'}^{M_N} \sum_{k=N-n-n'+2}^{N-n} \frac{W}{W-1} (W^{N-k+1} - W^{n'}) + (N-n')(n'-1) W^{n'} \right]. \end{aligned}$$

VI. REFERENCES

1. E. Masry and M. C. Lui, "Discrete-Time Spectral Estimation of Continuous Parameter Processes – A New Consistent Estimate," IEEE Trans Information Theory, vol IT-22, May 1976.
2. E. Masry, D. Klamer and C. Mirabile, "Spectral Estimation of Continuous Time Processes: Performance Comparison Between Periodic and Poisson Sampling Schemes," IEEE Trans Automatic Control, vol AC-23, August 1978.
3. F. J. Beutler, "Alias Free Randomly Timed Sampling of Stochastic Processes," IEEE Trans Information Theory, vol IT-16, 1970.
4. A. Papoulis, Probability, Random Variables and Stochastic Processes, New York: McGraw-Hill, 1965.
5. W. Gröbner und N. Hofreiter, INTEGRALTAFEL, Vol II, 1965, Springer-Verlag, Wien-New York.
6. G. Jenkins and D. Watts, Spectral Analysis and Its Applications, 1968, San Francisco: Holden-Day.